

# Effects of Friction and Disorder on the Quasi-Static Response of Granular Solids to a Localized Force

C. Goldenberg<sup>1,\*</sup> and I. Goldhirsch<sup>2,†</sup>

<sup>1</sup>*Laboratoire de Physique et Mécanique des Milieux Hétérogènes (CNRS UMR 7636), ESPCI, 10 rue Vauquelin, 75231 Paris Cedex 05, France.*

<sup>2</sup>*Department of Fluid Mechanics and Heat Transfer, Faculty of Engineering, Tel Aviv University, Ramat-Aviv, Tel Aviv 69978, Israel.*

(Dated: February 9, 2022)

The response to a localized force provides a sensitive test for different models of stress transmission in granular solids. The elasto-plastic models traditionally used by engineers have been challenged by theoretical and experimental results which suggest a wave-like (hyperbolic) propagation of the stress, as opposed to the elliptic equations of static elasticity. Numerical simulations of two-dimensional granular systems subject to a localized external force are employed to examine the nature of stress transmission in these systems as a function of the magnitude of the applied force, the frictional parameters and the disorder (polydispersity). The results indicate that in large systems (typically considered by engineers), the response is close to that predicted by isotropic elasticity whereas the response of small systems (or when sufficiently large forces are applied) is strongly anisotropic. In the latter case the applied force induces changes in the contact network accompanied by frictional sliding. The larger the coefficient of static friction, the more extended is the range of forces for which the response is elastic and the smaller the anisotropy. Increasing the degree of polydispersity (for the range studied, up to 25%) decreases the range of elastic response. This article is an extension of a previously published letter [1].

PACS numbers: 83.80.Fg, 45.70.Cc, 81.05.Rm, 46.65.+g

## I. INTRODUCTION

The description of the static phase of granular matter, much like its dynamical phases, is of significant current interest. Some studies focus on constitutive relations in order to describe the stress distribution in these materials whereas other investigations probe their microscopic characteristics, such as the nature of the force distributions and correlations.

Static and quasi-static properties of granular materials are commonly modeled by engineers using elasto-plastic [2, 3] and hypoplastic [4, 5] models. Other types of models have been put forward (mostly) by physicists. Some of these models comprise hyperbolic partial differential equations for the stress transmission through a granular material [6, 7, 8, 9, 10, 11]. This is in contrast with the elliptic, non-propagating nature of the classical equations of static elasticity. It seems that this dichotomy in the modeling of granular statics started [3, 12] in the context of the interpretation of experiments performed on conical piles [13, 14], where a pressure dip below the apex of the pile has been observed (the presence or absence of such a dip in conical piles and in wedges was found to depend on the construction method [15]).

In order to obtain insights into this problem it is convenient to consider the simpler geometry of a granular rectangular layer (or slab) resting on a solid support [16],

not the least since this class of systems is well researched experimentally [17, 18, 19, 20, 21, 22, 23]. Much like in the case of piles, the cited and other experiments seem to be sending mixed messages concerning the ‘correct’ description of stress transmission in granular slabs, as some render support to the elliptic descriptions whereas others are compatible with hyperbolic models. When the response to the application of an external force is linear in the force (for sufficiently small forces), the problem is tantamount to the study of the Green’s function of the system [22].

The present article is devoted to a detailed study of the response of two-dimensional vertical slabs comprising polydisperse frictional disks subject to gravity and a localized, compressive external load applied at the top of the slab; it expands upon the results of [1] in both content and detail.

The dependence of the response on the magnitude of the external force as well as the interaction parameters and degree of disorder (or polydispersity) is investigated. The results suggest a resolution of the above mentioned controversy as well as the seemingly mutually incompatible experimental results. First, noticing that strongly anisotropic elasticity can exhibit hyperbolic-like features (see more below) it is convenient to consider the response within the framework of elasticity. Note that it is not claimed that the process leading to a given state is elastic (often it is not) but rather that the excess stress field induced by an external force in a given (“prestressed”) static state can be described by the equations of elasticity and often even by linear isotropic elasticity (for an isotropic reference configuration), even in the pres-

\*Electronic address: chayg@pmmh.espci.fr

†Electronic address: isaac@eng.tau.ac.il

ence of friction (see also the recent elastic model reviewed in [24]). More specifically, large systems subject to “small” applied forces (which is likely to be the case in many engineering applications), can be described by isotropic elasticity except in the near vicinity of the point of application of the force (where one expects strong induced anisotropy and irreversible rearrangements). Sufficiently far from the point of application the external force leads to practically no sliding or rearrangement of the grains. The latter events are rarer the larger the friction and therefore, as shown below, the linearity and isotropy of the response are *enhanced* by friction.

Nonlinear/irreversible effects such as changes in the contact network and frictional sliding can naturally give rise to large *anisotropy*, yielding hyperbolic-like response (as already suggested in [3, 25]). In relatively small systems subject to sufficiently large forces, as in some experiments [17, 18, 21, 22, 23], the size of the nonlinear and anisotropic domain induced by the external forcing can be comparable to the system’s size, hence the stress transmission in such systems can be well described by hyperbolic or near-hyperbolic (see below) equations. Similar qualitative behavior is observed in both ordered (lattice) and disordered (polydisperse) configurations, the main difference being the range of magnitudes of external forces for which one observes elastic response.

Note that qualitatively similar results were obtained in a study of the *displacement* response rather than stress [26], using a similar numerical simulation. This study focused on the effect of the mean coordination number, controlled by the particle stiffness, rather than the effects of the frictional properties and the disorder which are the focus of the present work. Interestingly, an approach using a force network ensemble [27] also seems to yield qualitatively similar results concerning the effect of friction, although a full physical interpretation of this approach is still lacking.

The paper is organized as follows. Section II presents an outline of the elliptic (elastic) and hyperbolic descriptions of static granular matter and a comparison between the two. Results of some relevant experiments are reviewed in the same context. Sec. III provides a description of the simulation method. Sec. IV reports the results obtained for frictionless systems, and the subsequent sections describe more realistic simulations incorporating friction (Sec. V) and disorder (polydisperse systems, Sec. VI). The results of the simulations and their analysis enable the interpretation of the findings in different experiments: this comprises the content of Sec. VII. Sec. VIII offers a brief summary of the main results.

## II. ELLIPTIC VS. HYPERBOLIC DESCRIPTIONS

### A. Theoretical description

As mentioned, there are two main classes of models that have been proposed for the description of the response of granular assemblies. Broadly known as the “elliptic” and “hyperbolic” descriptions, their predictions differ both qualitatively and quantitatively. These respective predictions for the case of the response (excess pressure on the floor due to the external force, i.e., the pressure due to gravity in the otherwise unforced system is subtracted) to the application of an external vertical force at the center top of a slab are schematically illustrated in Fig. 1. The elliptic case is represented here by the results of *isotropic* elasticity [28]. In this case, a single peaked response on the floor is expected [Fig. 1(a)], its width being proportional to the depth (or height) of the slab. The shape of the peak is determined by the equations of elasticity, and depends on the boundary conditions at the floor [3, 20, 29] (e.g., its rigidity and roughness). In contrast, hyperbolic descriptions [6, 7, 8, 9, 10, 11] dictate that the stress propagates along characteristic directions, and two peaks are expected in 2D (a ring in 3D), their widths determined by diffusive broadening due to disorder [30] and (consequently) proportional to the square root of the depth of the slab. This type of description has been shown [7, 8, 9, 10, 11] to apply to (frictionless) isostatic systems [31, 32, 33], i.e., systems in which Newton’s first and third laws (and the boundary conditions) provide a number of equations that equals the number of unknowns (force components) thereby enabling the determination of the forces from these laws; it turns out these conditions determine an average coordination number for the particle contacts and that the latter is the minimum required to maintain the stability of the packing. This notion cannot be directly extended to hyperstatic systems (i.e., with a higher coordination number). The isostatic case is a marginally stable configuration, which may correspond to a plastic material which is everywhere at incipient yield (for which classical plasticity results in hyperbolic equations [3]). We also note that recent models based on the description of the stress in terms of propagating force chains which may split and merge [34, 35, 36, 37] have been shown to correspond to elastic-like equations at large scales [34, 35, 36]; a physical interpretation of the fields satisfying these equations is still lacking.

It is important to note that, as already mentioned in [3, 25, 29], elastic systems can exhibit hyperbolic-like behavior. In [29], we used a simple 2D model in order to demonstrate this property, i.e., a triangular lattice of harmonic springs in which the spring constant for the horizontal springs,  $K_1$ , is different from that of the oblique ones,  $K_2$ . This model corresponds (in the continuum limit) to an anisotropic elastic system (the response of an anisotropic elastic infinite half-plane (2D) with uniaxial

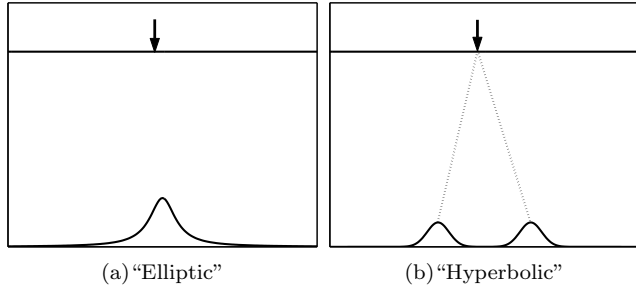


FIG. 1: Predictions of different models for the response of a granular slab to a localized vertical force applied to its top: pressure distribution on the floor supporting the slab.

symmetry has been analyzed in detail in [36]). The qualitative nature of the response depends on the degree of anisotropy: it is single peaked for values of  $K_2/K_1$  near 1 ( $K_2/K_1 = 1$  corresponds to an isotropic system). The response is narrower than the isotropic one for  $K_2/K_1 < 1$  and wider for  $K_2/K_1 > 1$ . For sufficiently large values of  $K_2/K_1$ , the response becomes double peaked, i.e., in qualitative agreement with the predictions of the hyperbolic models. However, the equations of anisotropic elasticity are elliptic, except in the extreme anisotropic limit  $K_2/K_1 \rightarrow \infty$  in which the equations do become hyperbolic. This is consistent with the fact that the limit  $K_1 \rightarrow 0$  corresponds to the absence of horizontal springs, and is therefore *isostatic*. This limit is similar to the case of a square (or cubic) lattice of springs which (to linear order in the displacement) has no shear rigidity along the lattice directions [38]. Although this anisotropic model seems quite artificial, we show below that anisotropy arises quite naturally in more realistic descriptions of granular materials.

## B. A Review of Experimental Results

This Section reviews some of the experiments in which the response of a granular slab to a localized force was measured.

In the experiments described in [18, 22], a localized vertical force was applied to a two-dimensional (2D) packing of photoelastic particles. Recall that stressed photoelastic solids viewed through cross-polarizers exhibit fringes whose density is proportional to the difference between the two principal values of the internal particle stress [39]. In the described experiment the applied forces had to be sufficiently large in order to observe the fringes; in practice forces that were about 150 times the particle weight were used. The stress is concentrated at the interparticle contacts. Post-processing techniques were used to extract the magnitudes of the interparticle forces from the experimental images [18, 22, 39]. Force chains were prominent in all studied realizations.

Three different types of packings were studied in [18,

22]. The most ordered was that of a triangular lattice of nominally monodisperse (equal) disks; less order was found in a packing of bidisperse disks (two different sizes), and a packing of pentagonally shaped particles was the most disordered of the three. The images from 50 configurations were averaged [18, 22] for each type of packing. The force profiles as a function of the horizontal (orthogonal to gravity) coordinate were plotted for different depths in each of the slabs [18, 22]. These profiles exhibited strong dependence on the particle shapes: the ordered lattice of monodisperse disks exhibited two prominent “force chains” along the lattice directions ( $60^\circ$  with respect to the horizontal), a result which appears to be consistent with a hyperbolic model of propagating forces (note, however, that a vertical force chain can be observed as well, and it is not anticipated by these models). As the disorder is increased, the force chains “fade out”, and for the random configuration of pentagonal particles in 2D the measured force profile possessed a single peak, the width of which varied linearly in the depth; the latter result is compatible with the predictions of elasticity. It was proposed that granular materials may experience a crossover from a hyperbolic to an elliptic behavior as the degree of disorder increases [18].

In another experiment, in which a rather small system was studied (of about 10 diameters in height), the slab comprised round-edged rectangular 2D particles [17]. In this case, the response appeared to exhibit a parabolic envelope. This type of force profile was predicted on the basis of models that assume an uncorrelated, diffusive propagation of the forces, such as the q-model [40, 41] (which was originally proposed to describe the statistics of force fluctuations). However, as mentioned, this system is quite small in terms of the number of constituents; furthermore, even in this case, it appears that the envelope may be narrowing down near the bottom of the slab. We shall return to the issue of system size below.

In the simulations reported in [23] the *displacement* (rather than the force) response of a 2D packing of disks of three different diameters was measured (in response to a small displacement of a particle at the bottom of the packing). The displacement response is expected to be qualitatively similar to the force response (in isostatic systems the two are equivalent [31, 32]). The measured response (averaged over several hundred configurations) is single peaked, and the width of the peak appears to grow as the square root of the height for small system heights, and cross over to a linear dependence at larger heights (the total height of the packing was about 10 diameters, which is quite small). The response function (scaled by the width) is fit quite well by a Gaussian. The same paper [23] presents simulations of isostatic systems which show, as expected, a double peaked response.

In the experiments described in [19, 20], an external localized force was applied at the top of 3D disordered slabs of sand (and other materials), and the response force profiles (i.e., the actual forces minus the corresponding forces without the external load) on the floor were measured.

In this case the applied force was rather small (a few particle weights), and the response was verified to be linear in the applied force. The measured response was single peaked, the profile width being proportional to the slab depth, as expected for an elastic system. However, the shape of the response was found to depend on the preparation method: it was wider for loose packings (obtained by pulling a sieve through the packing) than for dense packings (obtained by filling the container layer by layer, pressing the packing after each layer is deposited). The response could not be fitted by isotropic elastic solutions for finite slabs [20].

Unlike the highly disordered systems used in [18, 22], the experiments reported in [21] concerned ordered 3D close-packed systems of spherical particles, arranged on FCC (Face-Centered Cubic) and HCP (Hexagonal Close-Packed) lattices [42]. The forces on the floor were measured using pressure marks on carbon paper [21]; the applied forces used in these experiments were quite large (a few *thousand* times the particle weight). The results were averaged over several packings of nominally equal spheres. For shallow systems, three distinct peaks were observed in the case of the FCC lattice, and a sharp ring for the HCP lattice. This is consistent with a description based on propagating forces [21] (which would correspond to a hyperbolic continuum description). However, for larger systems the peaks were considerably less distinct, the response being ‘smoother’. This further indicates that a hyperbolic-like response may apply only to relatively small systems. For disordered (amorphous) packings [21], a single peak was obtained (a force impulse was used, since a large persistent force resulted in major rearrangements in the packing).

In summary, qualitatively different types of response to an external force were observed in experiments on granular assemblies, some of which seem to render support to elliptic models, others to hyperbolic or parabolic models of stress transmission. The degree of disorder seems to play an important role, as do the size of the system and the magnitude of the applied force. The observed differences also suggest that other parameters, such as the coefficient of friction, may be important. In order to clarify the role of these parameters and the associated physical mechanisms, we performed extensive simulations of 2D granular slabs, as described below.

### III. SIMULATION METHOD

In order to study the response of granular packings and its dependence on the particle properties in more detail, we employ the discrete element method [43, 44] (DEM), a particle-based simulation method for granular materials also known as the molecular dynamics (MD) simulation method [45, 46, 47, 48]. This method has been employed in studies of atomic and molecular assemblies as well as granular systems, see, e.g., [49, 50, 51]) for recent reviews. In the present work, DEM simulations

have been employed to study 2D systems composed of disks. The equations of motion for each particle are integrated using the Beeman algorithm [46], which provides more accurate velocities than the commonly used Verlet algorithm [46]. We verified that the use of a Gear 5-value predictor-corrector algorithm [48] does not result in any significant changes in the results.

#### A. The Force Model

Models for the interactions among solid grains are usually based on contact mechanics [52, 53]. Following the work of Hertz (see, e.g., [28]) and others, it is customary to assume that the forces exerted by solid particles on each other are pairwise additive. Since for relatively rigid particles the typical deformation of a particle is a very small perturbation to its shape and size, it is common to model these interactions as follows: the particles are fixed in shape and can overlap and the corresponding normal forces (perpendicular to the plane of contact among particles) are taken to be functions of the degree of this imaginary overlap. The tangential interparticle forces are taken to depend on the particles’ rotations as well.

Most natural or industrial granular materials comprise non-spherical particles. However, the latter are difficult to treat theoretically, and only few models for simulating their behavior have been suggested and studied (e.g., [54, 55, 56, 57, 58, 59]). Therefore the present paper specializes to disk shaped particles in two dimensions. The force model we use is essentially the same as that employed in [43] (for some other examples of force schemes commonly used in simulations, see, e.g., [60, 61, 62]).

For spherical or disk-shaped particles, the overlap of two particles is defined by:

$$\xi_{ij} \equiv R_i + R_j - |\mathbf{r}_{ij}|, \quad (1)$$

where  $R_i, R_j$  are the radii of the particles,  $\mathbf{r}_i$  is the position of the center of mass of particle,  $i$ , and  $\mathbf{r}_{ij} \equiv \mathbf{r}_i - \mathbf{r}_j$ . In noncohesive granular materials, the particles are assumed to interact only when they overlap, i.e., when  $\xi_{ij} > 0$ . For two frictionless elastic spheres, a classical result by Hertz (see, e.g., [28]) is that the force is proportional to  $\xi_{ij}^{3/2}$ , while for cylinders, it is linear in  $\xi_{ij}$  (up to a logarithmic correction, see, e.g., [63, 64]). In the simulations whose results are presented below the normal component (parallel to  $\mathbf{r}_{ij}$ ) of the force is taken to be linear in the overlap (linear spring); this choice is not due to the fact that we consider cylindrical particles, but rather in order to simplify the application of theoretical considerations. It may be further justified by the fact that we consider small deformations, in which case one may linearize the force-displacement law around a reference configuration [65].

Even for frictionless particles there can be dissipation, e.g., due to viscoelastic normal forces that depend

on the normal relative velocity  $\dot{\xi}_{ij}$  (see, e.g., [64, 66]). While hysteretic, rate independent dissipation models (see, e.g., [62, 67, 68]) may be more realistic than viscoelastic models, their implementation is more complicated. Since we focus on the static response and small deformations the results should not be sensitive to the precise choice of dissipation mechanism. We therefore use a damping term which is linear in the relative velocity of interacting particles (linear dashpot). All in all the normal interparticle force exerted by particle  $j$  on particle  $i$ ,  $\mathbf{f}_{ij}^N$ , can be expressed as:

$$\mathbf{f}_{ij}^N = (k_N \xi_{ij} + \nu_N v_{ij}^N) H(\xi_{ij}) \hat{\mathbf{r}}_{ij}, \quad (2)$$

where  $\hat{\mathbf{r}}_{ij}$  is the unit vector in the direction of  $\mathbf{r}_{ij}$ ,  $v_{ij}^N \equiv (\mathbf{v}_i - \mathbf{v}_j) \cdot \hat{\mathbf{r}}_{ij} \equiv \mathbf{v}_{ij} \cdot \hat{\mathbf{r}}_{ij}$  is the relative normal velocity of the particles,  $\nu_N$  is a fixed damping constant, and  $H(x)$  is the Heaviside function,

$$H(x) \equiv \begin{cases} 1 & x > 0 \\ 1/2 & x = 0 \\ 0 & x < 0 \end{cases}. \quad (3)$$

Next, consider the friction-induced tangential forces. A simple model for friction [43] includes tangential springs for modeling static friction, often with velocity-dependent damping to facilitate relaxation to a static configuration. The springs are generated at zero length, which is also their rest length, when two particles come into contact and “snap” when the resulting frictional force,  $f^T$ , satisfies  $f^T > \mu_S f^N$ , i.e., when the Coulomb limit is exceeded. Once a tangential spring is severed, the corresponding particles are allowed to slip with respect to each other and experience dynamic friction,  $f^T = \mu_D f^N$ . Note that the description of static friction in terms of a tangential spring is physically reasonable, and consistent with both contact mechanics on the macroscopic scale [52, 53] and microscopic approaches to the description of friction (see, e.g., [69] for a list of references on friction). The tangential springs are of course quite stiff, giving rise to very small, but measurable [70] displacement prior to slip. Tangential springs have often been used to model interparticle interactions in mean-field derivations of granular elasticity [71, 72, 73, 74]. More realistic descriptions of frictional contacts account for the history of contact deformations (see, e.g., [60, 61, 62, 67]).

The above tangential spring-dashpot model in conjunction with Coulomb’s law of friction serve as the basic tangential force law in the present work, as in [43]. For simplicity, the coefficients of static and dynamic friction are taken equal each other:  $\mu_D = \mu_S = \mu$  (the value of  $\mu_D$  does not directly affect the static configurations which are the main concern in the present work, although it may influence the evolution towards these states). In order to employ a tangential spring-dashpot force model, a relative tangential displacement has to be defined at each contact. To this end, note that the relative tangential velocity of two disks (in 2D) is given by:

$$\mathbf{v}_{ij}^T = \mathbf{v}_{ij} - v_{ij}^N \hat{\mathbf{r}}_{ij} - \hat{\mathbf{t}}_{ij} (R_i \omega_i + R_j \omega_j), \quad (4)$$

where  $\omega_i \equiv \dot{\theta}_i$  is the angular velocity and  $\hat{\mathbf{t}}_{ij} \equiv \hat{\mathbf{z}} \times \hat{\mathbf{r}}_{ij}$ . In the model used in this work the force exerted by a tangential spring depends on the relative tangential displacement,  $\mathbf{s}_{ij}$ , and is given by:

$$\mathbf{f}_{ij}^T = (-k_T \mathbf{s}_{ij} - \nu_T \mathbf{v}_{ij}^T) H(\xi_{ij}),$$

where  $k_T$  is the tangential spring constant and  $\mathbf{s}_{ij}$  obeys the following equation:

$$\dot{\mathbf{s}}_{ij} = [\mathbf{v}_{ij}^T + (\dot{\mathbf{s}}_{ij} \cdot \hat{\mathbf{t}}_{ij}) \hat{\mathbf{t}}_{ij}] H(|\mu \mathbf{f}_{ij}^N| - k_T |\mathbf{s}_{ij}|),$$

which ensures that the spring is always tangent to the plane of contact (a line in 2D), and does not exceed the length that corresponds to the Coulomb limit. In addition,  $\mathbf{s}_{ij}$  is set to zero if there is no overlap (i.e.,  $\xi_{ij} < 0$ ). In practice, the tangential displacement is obtained by integrating the relative tangential velocity from the time the particles establish contact. When  $\mu \mathbf{f}_{ij}^T > \mathbf{f}_{ij}^N$ , the length of the tangential spring is kept fixed in order to prevent the frictional force from exceeding the Coulomb limit. This is important in order to avoid unrealistic behavior when the contacts cease “sliding” (i.e.,  $f^T = \mu f^N$ ), and revert to “sticking” ( $f^T < \mu f^N$ ) [75]: if the integration of the tangential velocity is continued for a sliding contact, and the result used to further stretch the tangential spring, the result will be an unrealistically large force when the contact reverts to sticking. Note that the torques exerted on the particles determine their angular accelerations; the corresponding equations are part of the system of equations that are solved.

The interactions of the particles with the walls are similar to the interparticle interactions. Since the walls considered here are rigid and fixed straight lines (in 2D), the overlaps are calculated accordingly, with the same force models. The force constants for particle-wall interactions ( $k_N^{\text{wall}}, k_T^{\text{wall}}, \nu_N^{\text{wall}}, \nu_T^{\text{wall}}, \mu^{\text{wall}}$ ) may be specified to be different from those used for particle-particle interactions (which are taken to be the same for all particle pairs).

In addition to interparticle forces and particle-wall forces, the force laws account for gravity. External forces and torques may also be applied to specific particles (see below).

## B. Simulation Parameters

The systems studied here consist of collections of poly-disperse disks, whose radii are uniformly distributed in the interval  $[R - \delta \cdot R, R]$ . In order to facilitate the use of parameters from experiments performed on short cylinders, the cylinder thickness,  $W$ , and its volume density,  $\rho$ , are specified, and the particle masses are given by  $m_i = \pi R_i^2 W \rho$ . We consider the case of homogeneous disks, for which the axial moment of inertia is given by  $I_i = \frac{1}{2} m_i R_i^2$ . The parameters used in this work correspond to experiments performed by the Duke group using 2D photoelastic disks [76]:  $R = 3.75 \cdot 10^{-3}$  m;  $W = 6.6 \cdot 10^{-3}$  m;  $\rho = 1.15 \cdot 10^3$  kg/m<sup>3</sup>.

The simulation results are presented in terms of non-dimensional quantities defined as follows. The length unit is the mean particle radius  $\bar{R}$ , the time unit is  $\tau = \sqrt{\bar{R}/g}$  (where  $g$  is the magnitude of the acceleration of gravity) and the mass unit is the mean particle mass  $\bar{m}$ . In simulations which account for gravity, we use  $g = 9.8\text{m/s}^2$ .

The normal spring constant used for particle-particle interactions is  $k_N = 3000\bar{m}g/\bar{R}$ . This value is based on force-displacement measurements performed on the photoelastic disks mentioned above [65]. Although the particles are cylindrical, measurements showed a force proportional to the  $\frac{3}{2}$  power of the displacement (possibly indicating that the contact area is elliptic rather than rectangular). For the typical deformations obtained in the experiments, a linear fit to the particle force law provides quite a good description [65], which further justifies our choice of modeling the normal force as that exerted by a linear spring with the above mentioned effective spring constant. For particle-wall interactions, we use  $k_N^{\text{wall}} = 2k_N$ .

The damping coefficient is typically chosen to correspond to half the critical damping value for an individual contact,  $\nu_c = 2\sqrt{k}$  (recall that  $k$  and  $\nu$  are non-dimensional), i.e., we use  $\nu_{N,T} = \sqrt{k_{N,T}}$ . This value was found to produce the fastest relaxation of the system towards static equilibrium and is irrelevant in the state of mechanical equilibrium itself.

The time step used in the simulations was  $\Delta t = 5 \cdot 10^{-4}\tau = 5 \cdot 10^{-4}\sqrt{\bar{R}/g}$ . We verified that decreasing the time step did not affect the results of the simulations.

Other simulation parameters such as the ratio  $k_T/k_N$  (and  $k_T^{\text{wall}}/k_N^{\text{wall}}$ , which is taken to equal it), the coefficients of friction  $\mu, \mu^{\text{wall}}$  and the polydispersity  $\delta$  were varied in different runs, and their influence is discussed below.

### C. Initial Conditions and Simulation Procedure

The initial configuration is produced by placing the particles on a triangular lattice with lattice constant  $2\bar{R}$ . The side walls and the floor are placed at a distance  $\bar{R}$  from the centers of the particles closest to the walls (so that for a monodisperse packing,  $R_i = \bar{R}$ , these particles are tangent to the side walls and the floor). The initial (translational and angular) velocities for all particles are set to zero. The system is then allowed to relax under gravity until it reaches static equilibrium, as described below.

In order to study the response to a localized force, the resulting configuration (with all velocities, translational and angular, reset to zero) is used as an initial configuration for a second run of the simulation, in which an additional external force (and/or an external torque in some simulations) is applied to a particle at the center of the top row of particles. The force is increased linearly

in time from zero to its desired value. The system is then relaxed again to static equilibrium.

The main criterion used for testing whether the system has reached static equilibrium (at which time the simulation is stopped) is the kinetic energy per particle. We found that in order to obtain an accuracy of less than 1% for the forces on the floor in a given realization, which are used here to define the response of the system to a localized force, the system has to be relaxed to a kinetic energy of  $E_k^{\text{stop}} = 10^{-13}\bar{m}g\bar{R}$  per particle, which is significantly smaller than that used in previous studies (e.g., in [77], the systems are relaxed to  $E_k^{\text{stop}} = 2 \cdot 10^{-8}\bar{m}g\bar{R}$  per particle). For polydisperse systems the response was coarse grained and averaged over a number of different configurations (Sec. VI), since the forces exhibit strong fluctuations. In this case, sufficient accuracy was obtained with  $E_k^{\text{stop}} = 10^{-9}\bar{m}g\bar{R}$ . We verified that several other criteria for static equilibrium (see [78]) were satisfied: the contact network was fixed for at least several hundred time steps (and each particle had at least two contacts), there were no sliding contacts, and the mean particle acceleration was less than  $10^{-5}\bar{m}g$ . For friction-

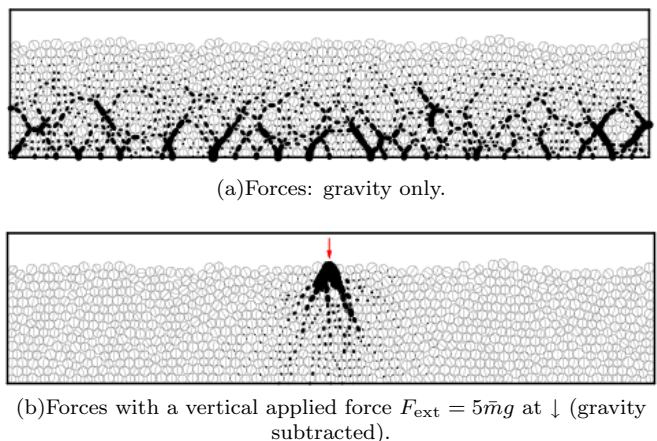


FIG. 2: Forces obtained in a DEM simulation of a polydisperse ( $\delta = 0.25$ ) frictional system with  $k_T/k_N = 0.8$ ,  $\mu = \mu^{\text{wall}} = 0.2$ . The line widths and lengths are proportional to the force magnitudes. (a) After relaxation under gravity, (b) After relaxation with an additional vertical force  $F_{\text{ext}} = 5\bar{m}g$ , where  $\bar{m}$  is the mean particle mass, with the forces obtained in (a) subtracted. The lines drawn inside the particles indicate the rotation angles: in the initial configuration for the simulation (before the relaxation under gravity) the lines are vertical. An arrow denotes the position of the externally applied force.

less systems ( $\mu = \mu^{\text{wall}} = 0$ ), we found that reaching such small energies in a reasonable simulation time was very difficult due to the existence of slow global modes with a low dissipation rate, so that the following algorithm was used for accelerating the relaxation: the MD simulation was stopped at a higher energy ( $E_k^{\text{stop}} = 10^{-6}\bar{m}g\bar{R}$ ). The configuration obtained at this stage was used as a reference state around which (since the interactions are harmonic in the static case) the linearized equations of

motion were used iteratively to obtain a system which is closer to static equilibrium. In each iteration the equations were solved by matrix inversion, and the connectivity of the particles was updated to ensure that there was no tension. The iterations were stopped when the maximal relative particle displacement was less than  $10^{-14}\bar{R}$  (which is essentially the numerical accuracy). The typical kinetic energy obtained when using the resulting configuration as an initial configuration for the full DEM simulation was less than  $E_k = 10^{-22}\bar{m}g\bar{R}$  per particle. This configuration was then used for calculating the interparticle forces.

An example of the interparticle forces obtained in a typical simulation run is presented in Fig. 2. In order to calculate the response to an applied force, the forces due to gravity alone (without the applied force) are subtracted (vectorially) at each contact.

#### IV. RESPONSE OF FRICTIONLESS SLABS

Consider first frictionless particles, interacting by unilateral (“one-sided”) springs, which apply force only when compressed, modeling repulsive-only particle interactions [29], see Eq. (2). As shown in [29], the application of a localized force at the top of the packing can lead to rearrangements in the contact network: horizontal springs in the region below the point of application of the force are opened (as also observed in [79] for a pile geometry). The force chains in this system are qualitatively similar to those obtained with regular (“two-sided”) springs. However, the force magnitudes vs. the horizontal coordinate at different depths are expectedly in better agreement with experiment in the case of one-sided springs [18, 22] than that of regular springs [29], since the former model is more realistic for granular systems. The stress distribution obtained for unilateral springs [29] is anisotropic, and shows two peaks at the floor. This anisotropy is obviously related to the existence of a region of open horizontal contacts where the anisotropy is large and the hyperbolic limit applies [29]. This anisotropy is not present in the system without the application of the external forces; it is induced (through the changes in the contact network) by the applied force [29]. The induced changes in the contact network obviously qualify as a nonlinear process.

These changes in the contact network may be modeled as a nonlinear extension of the linear elastic continuum behavior obtained in a network of harmonic springs. While the (possibly position-dependent) elastic moduli in linear elasticity are time-independent material properties, a possible extension is to introduce a stress history dependence of the elastic moduli (i.e., the anisotropy induced by the opening of contacts in certain regions may be considered a result of an attempted tensile stress in those regions). A similar type of stress-induced anisotropy has been suggested in the context of plastic models of soil mechanics [80] as well as in nonlinear elas-

tic models [24]. If the particle positions do not change significantly, so that only the contact network is modified in response to the applied stress, the behavior can possibly be modeled as “incrementally elastic”. Under certain conditions (corresponding to plastic yield), the system is no longer able to support the applied stress without a major rearrangement of the particles. Incipient plastic yield may be related to a local extreme anisotropy typical of a marginally stable isostatic configuration.

##### A. Dependence on the Applied Force: Crossover from Hyperbolic-Like to Elliptic Response

In order to examine the changes in the contact network in more detail, we performed DEM simulations, as described in Sec. III, of a system similar to those discussed in [29], with different applied forces. We focused on systems of 15 layers of 60 particles each; the effect of system size is discussed below. The force response on the floor (subtracting the effect of gravity) is shown in Fig. 3. A crossover from a single peaked to a double peaked response occurs as the applied force is increased. The changes in the contact network corresponding to

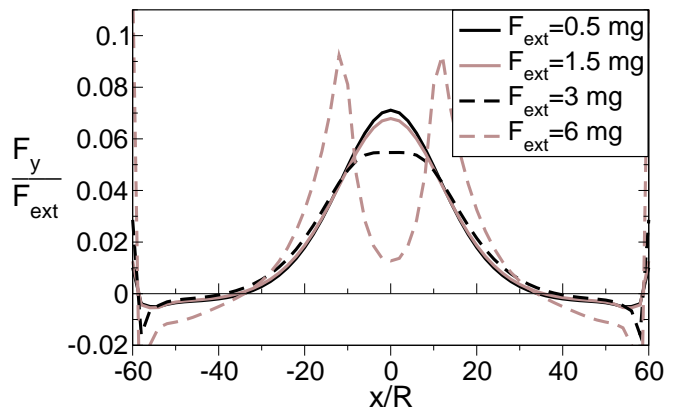


FIG. 3: The response of frictionless ordered systems for different applied forces,  $F_{\text{ext}}$ .

the systems of Fig. 3 are shown in Fig. 4. For a sufficiently small force (not shown), the contact network is unchanged, and the response is fully elastic (see Sec. V for a discussion of the linearity of the response). As the force is increased, horizontal contacts are opened in a teardrop shaped region below the point of application of the force, whose size increases with the force and decreases with friction. As mentioned above, in this region the extreme anisotropic limit of elasticity applies. When the “teardrop” is sufficiently far from the floor [Fig. 4(a)-(b)], the response at the floor is single peaked, as the changes induced by the force can be considered to be localized. Otherwise, the anisotropy induced by the external force reaches the floor (Fig. 4(c), inducing a double peaked response (the crossover actually occurs at slightly smaller forces, at which the “teardrop” almost



reaches the floor).

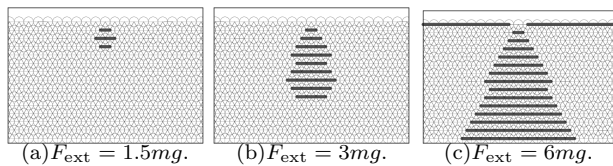


FIG. 4: Changes in the contact network in an ordered frictionless system for different applied forces. The central third of the system is shown. Thick lines connecting particle centers indicate contacts opened due to the application of the force; thin black lines represent contacts which are unaffected by the external force.

### B. Dependence on System Size

The dependence of the crossover on the size of the system is important for the interpretation of experimental results. The depth and maximal width of the “teardrop” as a function of the applied force, for several system sizes, are plotted in Fig. 5. As the “process” of opening of contacts with increasing applied force is nonlinear (since the effective elastic properties of the system are modified in the process), it is difficult to model it analytically. However, Fig. 5 clearly demonstrates that the size of the “teardrop” only slightly decreases as the depth of the slab increases.

This indicates that for large systems (as typically found in nature and in engineering application), this change in the contact network gives a finite size correction to the response [1]. For identical external loads, very deep systems should exhibit a single peaked response whereas relatively shallow ones, as studied in some experiments (Sec. II B), should exhibit two peaks. This is the main reason that different experiments, using differently sized samples, yield qualitatively different results. This observation also applies when frictional interactions are accounted for, as described in Sec. V.

### C. Dependence on Particle Stiffness

It is clearly important to consider the effect of the stiffness of the particles. We performed simulations with different values of  $k_N$ , and found that the size of the “teardrop” did increase with the stiffness of the particles, but appeared to saturate for  $k_N \gtrsim 2000mg/R$ . The results presented here pertain to  $k_N = 3000mg/R$ . The response is also quite insensitive to the choice of stiffness for  $k_N \gtrsim 1000mg/R$ : at  $x = 0$ , it only changes by about 2% in the range  $1000mg/R < k_N < 10^5mg/R$ . We conclude that the crossover from a single peaked to a double peaked response is essentially independent of the particle rigidity (provided that the particles are sufficiently stiff; otherwise the particle “overlaps” may be

appreciable and the localized force would lead to significant rearrangements of the particles).

The independence on the particle stiffness may be understood as follows: in the reference configuration, contacts are compressed due to gravity as well as the rigid walls and floor, i.e., the stress, and in particular its component parallel to the horizontal contacts,  $\sigma_{xx}$ , is compressive (the same condition may of course be obtained by applying an external pressure to the system). The external force acts in the opposite direction, i.e., it attempts to give rise to tensile forces. Therefore, the opening of contacts is due to a “competition” between the compression due to gravity and the tensile (excess) forces due to the applied force, and is therefore determined directly by the stress, rather than the strain (which does depend on the particle stiffness, of course), provided that the geometry is not significantly affected by the applied force (as it would for particles which are sufficiently soft to allow significant overlap). This justifies our choice of the particle weight as the unit of force (rather than a scale based on the particle stiffness and size). The same behavior may persist even in the limit  $k_N \rightarrow \infty$  under the same boundary conditions provided that the particles in the reference state are still in contact along the horizontal direction. However, as the stiffness increases, this requirement may be hard to comply with, as the particles must fit exactly between the walls in order to remain in contact: in the limit  $k_N \rightarrow \infty$  most horizontal contacts may be absent already in the reference state, rendering it isostatic (therefore, extremely anisotropic), and this would lead to a hyperbolic-like response even for an infinitesimal applied force, as suggested in, e.g., [7, 8, 9, 10, 11]. Therefore the above ‘limit of infinite stiffness’ should be understood as ‘large but finite’ stiffness else isostaticity comes into play. Furthermore, one must bear in mind that frictionless particles are a rather artificial idealization in the context of granular materials. Indeed, as we show in the next section, the presence of friction affects the behavior of the system very significantly and, in particular, renders it much less sensitive to the contact network.

## V. EFFECTS OF FRICTION

### A. Dependence on the Applied Force: Friction Increases the Linear Range

As mentioned in Sec. IV, for sufficiently small external forces no changes are induced in the contact network, so that the response is expected to be linear in the applied force [81]. This is shown in more detail in Fig. 6, which presents the response at the floor (vertical force on the floor) at  $x = 0$  (below the point of application of the force) as a function of the applied force, in both frictionless and frictional systems (with  $k_T/k_N = 0.8$ ; the effect of this parameter is discussed below). The results shown here were obtained with frictionless walls ( $\mu^{\text{wall}} = 0$ ; see Sec. III), since for weak applied forces, frictional walls can



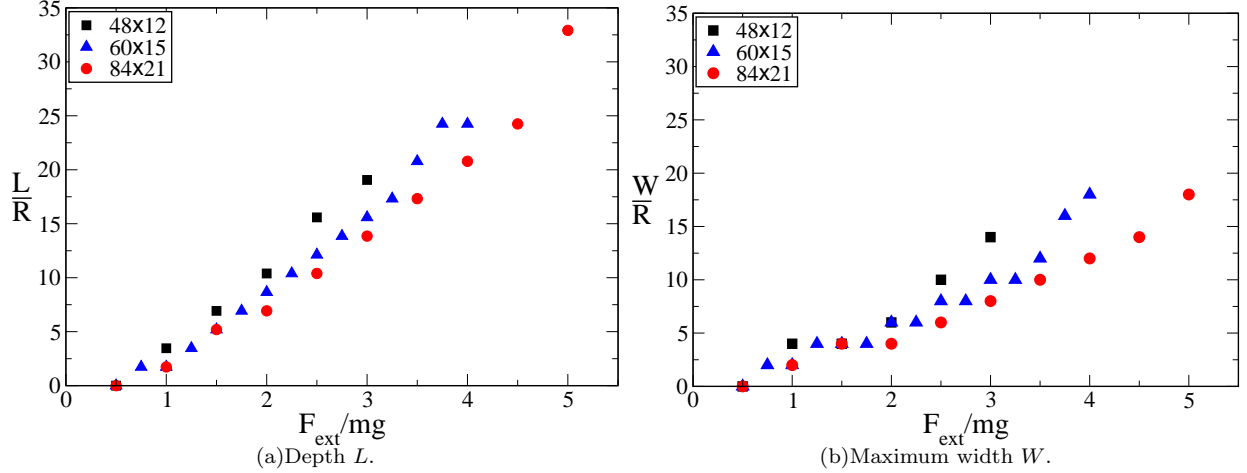


FIG. 5: The depth and maximal width of the “teardrop” in units of the particle radius,  $R$ , in ordered (monodisperse) frictionless systems (Fig. 4), as a function of the applied force, normalized by the weight of a particle, for different system sizes.

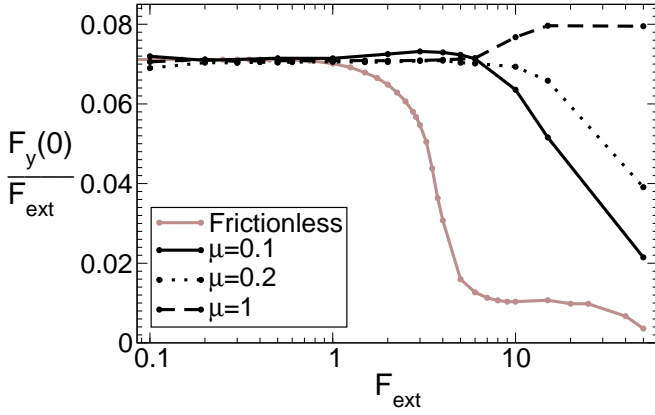


FIG. 6: The response at  $x=0$  of ordered systems, normalized by the applied force,  $F_{\text{ext}}$ , vs. the applied force (given in units of the particle weight,  $mg$ ), for different coefficients of friction  $\mu$ , frictionless walls ( $\mu^{\text{wall}}=0$ ) and  $k_T/k_N=0.8$ .

support some of the force, inducing nonlinearity in the response at the floor. A linear (*elastic*) range is observed for a sufficiently small applied forces *even for frictionless particles*, due to the fact that the particles are slightly deformed by gravity, and a small force does not cause the contacts to open.

As shown in Fig. 6, friction has a significant effect on the linearity of the response: The extent of the linear range is significantly larger (by almost an order of magnitude; notice the logarithmic scale on the horizontal axis in Fig. 6) in frictional systems, so that elasticity is *enhanced by friction*.

The effect of friction on the response is shown in more detail in Fig. 7, which presents the response profile on the floor for different applied forces, for  $\mu=0.2$  and  $\mu=1$  (compare to the frictionless case presented in Fig. 3). Notice that the force for which the crossover from a sin-

gle peaked to a double peaked response occurs rapidly increases with friction (this is also observed in Fig. 6), so that friction renders the response closer to that expected from *isotropic* elasticity (this is further discussed below). For  $\mu=1$  no such crossover is observed even for the largest force shown,  $F_{\text{ext}}=50mg$  (a different type of crossover occurs for  $\mu=1$  for large forces, as described in Sec. V E). Note that much larger forces may induce major rearrangements (i.e., plastic flow), while our focus here is on the solid-like regime, in which the particle displacements are small.

## B. The Effect of Friction on the Contact Network

To gain a better understanding of the effect of friction on the response, we examine the changes in the contact network. We first recall that such changes occur at significantly larger applied forces in the frictional case (by almost an order of magnitude): the first contact is opened when  $F_{\text{ext}}=0.75mg$  in the frictionless case,  $F_{\text{ext}}=4mg$  for  $\mu=0.2$ , and  $F_{\text{ext}}=6mg$  for  $\mu=1$ . This is the origin of the extended linear range observed in frictional systems.

The effect of the applied force on the changes in the contact network in a system with  $\mu=0.2$  is shown in Fig. 8 (compare to Fig. 4). For the same force, the region of open contacts is considerably smaller in the frictional case than in the frictionless case [compare Fig. 4(c) and Fig. 8(a)]. In addition, this region reaches the floor only for a much larger force [compare Fig. 4(c) and Fig. 8(c)]. This may explain the fact that the crossover to a double peaked response occurs at larger forces in the frictional case, since this type of response is related to the anisotropy in this domain.

The above observations of the changes in the contact network seem to explain the effect of friction on the range

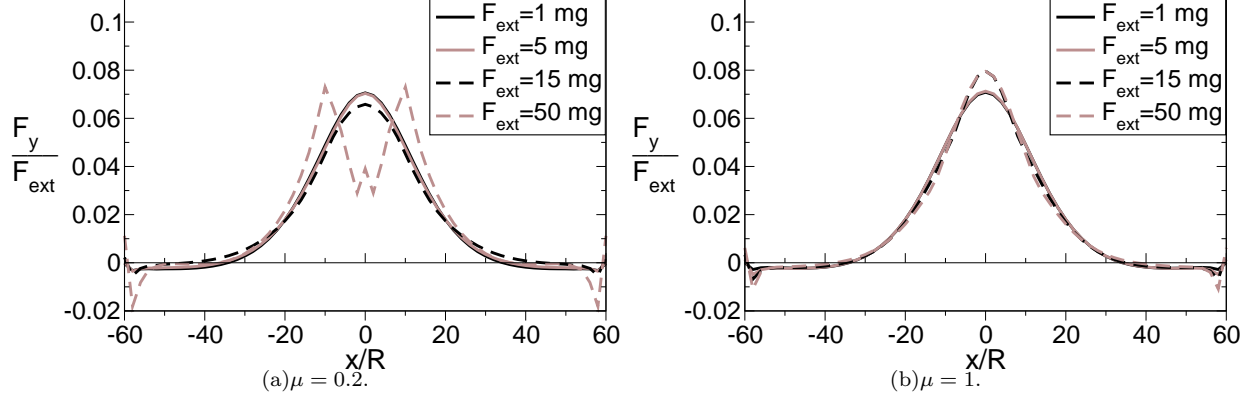


FIG. 7: The response of ordered systems, with different coefficients of friction  $\mu$ , to applied forces ( $F_{\text{ext}}$ ) of different magnitudes, frictionless walls ( $\mu^{\text{wall}} = 0$ ) and  $k_T/k_N = 0.8$  (compare to Fig. 3).

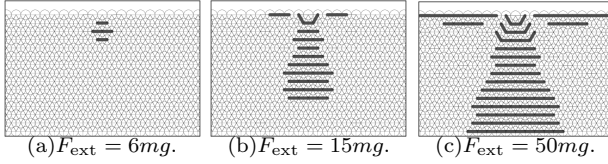


FIG. 8: Changes in the contact network in a frictional system with  $\mu = 0.2$ , with different applied forces  $F_{\text{ext}}$ , frictionless walls ( $\mu^{\text{wall}} = 0$ ) and  $k_T/k_N = 0.8$ . The various lines are explained in the caption of Fig. 4.

of linearity and magnitude of the crossover force. However, the source of this effect, namely, the reason for the smaller changes in the contact network in the presence of friction, still needs to be elucidated (see below). In addition, for a larger coefficient of friction, the obtained response does not seem to be compatible with the changes in the contact network: as mentioned above [see Fig. 7(b)], for  $\mu = 1$  the response remains single peaked (and actually its shape becomes sharper) even for rather large forces (see however Sec. V E), while for the same force, the response for  $\mu = 0.2$  is double peaked. The changes in the contact network for  $\mu = 1$  are shown in Fig. 9. While the region of open contacts does reach the floor (even for a smaller force than in the case of  $\mu = 0.2$ ), the response remains single peaked.

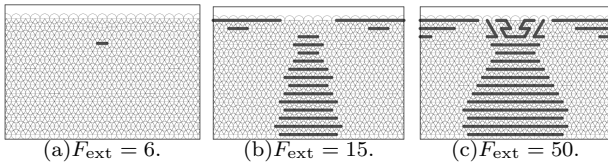


FIG. 9: Changes in the contact network in a frictional system with  $\mu = 1$ , with different applied forces  $F_{\text{ext}}$ , frictionless walls ( $\mu^{\text{wall}} = 0$ ) and  $k_T/k_N = 0.8$ .

The results obtained for  $\mu = 1$  suggest that in the

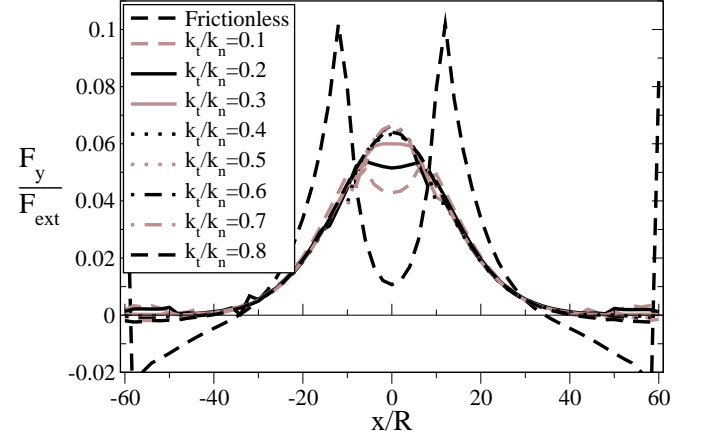


FIG. 10: The response of ordered systems for a large coefficient of friction ( $\mu = 10$ ) and different values of the ratio of tangential to normal stiffness,  $k_T/k_N$ , with  $F_{\text{ext}} = 15mg$ .

presence of friction, the anisotropy of the region of open contacts is greatly reduced (compared to the frictionless case). When  $\mu$  is sufficiently large (and  $F_{\text{ext}}$  sufficiently small), its value is essentially immaterial, since sliding is never reached. In this case, the ratio of tangential to normal stiffness,  $k_T/k_N$  (see Sec. III A), determines the response: Fig. 10 presents the response obtained with  $F_{\text{ext}} = 15mg$  for  $\mu = 10$  (which is practically equivalent to  $\mu = \infty$ , as used in [26], since no sliding occurs), with different values of  $k_T/k_N$ . A crossover from a single peaked to a double peaked response occurs with *decreasing*  $k_T/k_N$  (the crossover occurs at  $k_T/k_N \simeq 0.3$ ). For larger values of  $k_T/k_N$ , the response is nearly independent of  $k_T/k_N$ . This phenomenon is further studied immediately below.

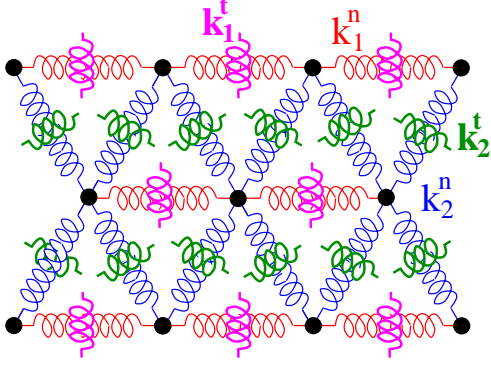


FIG. 11: A spring model with normal and tangential springs.

### C. A Model for Large Friction: the Role of Tangential Stiffness

In order to understand the dependence of the response on  $k_T/k_N$ , we consider a 2D spring network model similar to the one described in [29] (i.e., a triangular lattice with different spring constants for horizontal springs,  $k_1^n$ , and oblique springs,  $k_2^n$ ). In addition, this model (see Fig. 11) contains tangential springs (as used in our DEM simulations; Sec. III A), with spring constants which are different for horizontal,  $k_1^t$ , and oblique contacts,  $k_2^t$  [81]. Note that if one considers Hertzian interactions, the existence of anisotropic prestress (e.g., due to gravity) may indeed result in different spring constants in the horizontal and oblique directions. This model does not incorporate sliding, so that it corresponds to  $\mu = \infty$ . Similar models were studied in [71, 82, 83], and more recently in [36, 74, 84], where equal spring constants were used in all lattice directions.

The elastic moduli corresponding to the long-wavelength limit of this model can be calculated as follows: to leading order in the relative particle displacements  $\mathbf{u}_{ij}$  (which is the relevant order for linear elasticity), the elastic energy of the system is given by:

$$E^{\text{el}} = \frac{1}{2} \sum_{\langle ij \rangle} k_{ij}^n [\hat{r}_{ij} \cdot \mathbf{u}_{ij}]^2 + k_{ij}^t [\mathbf{u}_{ij} - (\hat{r}_{ij} \cdot \mathbf{u}_{ij}) \hat{r}_{ij}]^2, \quad (5)$$

where the sum is over nearest neighbors, and the values of  $k_{ij}^n$  and  $k_{ij}^t$  are taken according to Fig. 11 and the above description. In order to obtain the elastic moduli corresponding to the continuum limit of the considered system, an affine deformation (which is appropriate for a lattice configuration) is defined by a symmetric, uniform strain field:  $u_{ij\alpha}(\mathbf{r}, t) = \epsilon_{\alpha\beta} r_{ij\beta}$ . Note that when tangential forces are present, the stress is not necessarily symmetric (as assumed in classical elasticity); however, the micropolar terms due to this asymmetry are of higher order in the strain. We verified (in the DEM simulations) that they are very small, even near the point of application of the external force, where the magnitude of the

antisymmetric part of the stress is only a few percent of the pressure.

Using the notation of [36]:

$$E^{\text{el}} = \frac{1}{2} \begin{pmatrix} \epsilon_{xx} \\ \epsilon_{zz} \\ \epsilon_{xz} \end{pmatrix}^T \begin{pmatrix} a & c & 0 \\ c & b & 0 \\ 0 & 0 & d \end{pmatrix} \begin{pmatrix} \epsilon_{xx} \\ \epsilon_{zz} \\ \epsilon_{xz} \end{pmatrix}, \quad (6)$$

where the superscript, T, denotes the transpose, one obtains the following elastic moduli:

$$a = \frac{R^2}{2A} (8k_1^n + k_2^n + 3k_2^t) \quad (7)$$

$$b = \frac{R^2}{2A} (9k_2^n + 3k_2^t) \quad (8)$$

$$c = \frac{R^2}{2A} (3k_2^n - 3k_2^t) \quad (9)$$

$$d = \frac{R^2}{2A} (6k_2^n + 4k_1^t + 2k_2^t), \quad (10)$$

where  $A = 2\sqrt{3}R^2$  is the area of the unit cell. These results are consistent with those obtained in [36] for normal springs only, but different from the model with bending interactions introduced in [36].

In a domain of open horizontal contacts one has  $k_1^n = k_1^t = 0$ . It was already shown in Sec. IV that in the absence of tangential forces ( $k_2^t = 0$ ), this system corresponds to the extreme anisotropic limit. However, since the oblique tangential springs apply forces which have horizontal components, they can (at least partially) compensate for the absence of normal horizontal springs, and therefore significantly decrease the anisotropy.

Otto et al. [36] present continuum elastic solutions for an anisotropic infinite half plane subject to a localized force. They found a criterion for the elastic moduli at which a crossover occurs from a single peaked response to a double peaked one [36]: two peaks are expected for  $r \equiv \frac{1}{bd} [ab - c(d+c)] < 0$ . Note that this criterion refers to an infinite half-plane rather than a slab of finite width, which is more appropriate for describing our simulations. In addition, this model is homogeneous, while the region of open contacts (even when it reaches the floor) is roughly a triangle below the point of application of the force. Nevertheless, the estimate obtained using this criterion fits our result for the finite slab quite well: for the model used here (with no horizontal springs),  $r = \frac{\beta^2 + 10\beta - 3}{\beta^2 + 6\beta + 9}$ , where  $\beta \equiv k_2^t/k_2^n$ . Hence (in the physically relevant range  $\beta > 0$ ), two peaks are expected for  $\beta \lesssim 0.2915$ , which is consistent with the value  $k_T/k_N \simeq 0.3$  obtained in the simulation (Fig. 10).

For an infinitesimal tangential load applied to a system composed of elastic spheres, the Cattaneo-Mindlin model [53] yields  $k_T/k_N = \frac{2(1-\nu)}{2-\nu}$ , where  $\nu$  is the Poisson ratio of the spheres. For the range of positive Poisson ratios ( $0 \leq \nu \leq 0.5$ ; notice that this is a 3D Poisson's ratio), this implies that  $\frac{2}{3} \leq k_T/k_N \leq 1$ , so that the minimum value of  $k_T/k_N$  is well above the crossover from two peaks to one. In most of the simulations presented

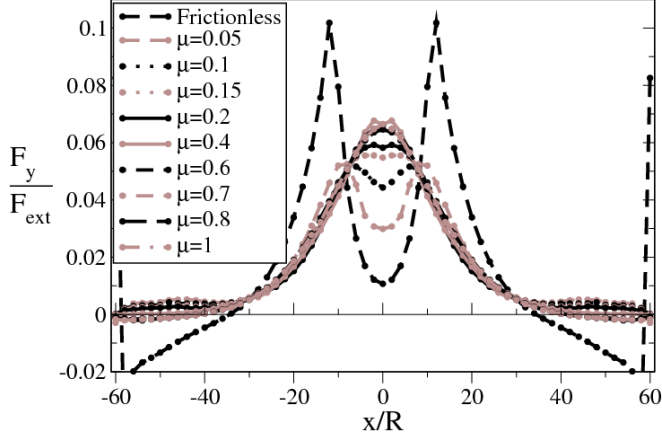


FIG. 12: The response of ordered systems for  $k_T/k_N = 0.8$  and different values of the coefficient of friction, with  $F_{\text{ext}} = 15mg$ .

in this work, we use  $k_T/k_N = 0.8$ , which corresponds to a realistic Poisson ratio of about 0.3.

#### D. More on the effects of friction

The above results show that static friction acts to retain an “effective connectivity” between the grains when the horizontal contacts are disconnected, and renders the system more isotropic than one would have naively anticipated. However, the frictional forces are limited by the Coulomb condition ( $f^T \leq \mu f^N$ ; see Sec. III A), so that if  $\mu$  is too small (or  $F_{\text{ext}}$  large), sliding occurs. This increases the anisotropy, since not all the tangential springs can exert forces as large as predicted by the above model (in which  $\mu = \infty$ ) and leads to a crossover to a double peaked response. This crossover is shown as a function of  $\mu$  (for  $F_{\text{ext}} = 15mg$ ) in Fig. 12.

In considering the effect of the coefficient of *static* friction, note that unlike the coefficient of *dynamic* friction, which is typically smaller than 1, the effective coefficient of static friction (which determines the onset of sliding) may be significantly larger than 1 even for rough spherical particles, and certainly for irregularly shaped particles (which can interlock and prevent their relative rotation).

The effects of friction are also evident in the forces (Fig. 13) as well as the vertical stress component  $\sigma_{zz}$  (Fig. 14), calculated using the expression presented in [29, 85]. In particular, the reduced anisotropy is apparent in the stress field (the stress field for  $\mu = 1$  is quite similar to that obtained in the case of an isotropic harmonic lattice [29]).

The most prominent effect of friction on the force chains (Fig. 13) is that the forces (and hence the chains) no longer need to be aligned with the (here, triangular) lattice direction, as they are in the absence of tangential forces. In particular, a vertical force chain is evident for  $\mu = 1$ . Such a chain is actually observed in the exper-

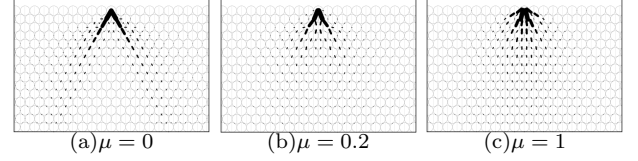


FIG. 13: The interparticle forces in ordered systems with different coefficients of friction ( $\mu^{\text{wall}} = \mu$ ,  $k_T/k_N = 0.8$ ), with  $F_{\text{ext}} = 15mg$ . The effect of gravity has been subtracted. The central third of the system is shown. Line widths and lengths are proportional to the force magnitude.

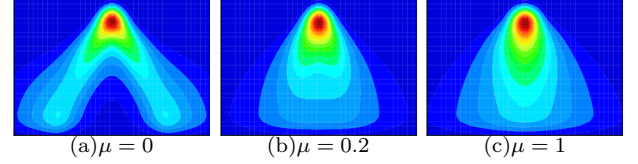


FIG. 14: The vertical stress  $\sigma_{zz}$  in the systems shown in Fig. 13, calculated using a Gaussian coarse graining function with a coarse graining width  $w = 2R$ . The effect of gravity has been subtracted.

iment [18, 22]. The inclusion of friction does provide a better fit to the experimental results obtained in [18, 22] for the monodisperse ordered packing: the force magnitudes vs. the horizontal coordinate at different depths in DEM simulations with frictionless and frictional ( $\mu = 1$ ; for the particles used in the experiments,  $\mu \simeq 0.94$  [76]) are shown in Fig. 15. We have also been able to reproduce [86] force chains along non-lattice directions observed in experiments with an applied force at oblique angles [22], using similar simulations of frictional particles (with some polydispersity; see Sec. VI below).

#### E. Symmetry Breaking for $\mu = 1$

As described above, for a relatively small coefficient of friction we observe a gradual crossover from a single peaked to a double peaked response as a function of the magnitude of the externally applied force, much like in frictionless systems, the main difference being that it occurs at larger values of the applied force [compare Figs. 3 and 7(a)], although the shape of the response is not identical. We reiterate that for the frictional case, this crossover can be explained as follows: in the limit  $\mu \rightarrow \infty$ , the induced anisotropy due the changes in the contact network (the opening of contacts; see Figs. 4 and 8) is compensated by the tangential forces, which renders the response single peaked for  $k_T/k_N \gtrsim 0.3$ . For finite  $\mu$ , this compensation is limited by the Coulomb condition, a limitation which becomes more significant as the applied force is increased: for  $\mu = 0.2$ , the region of open contacts (the “teardrop”) reaches the floor for  $F_{\text{ext}} \simeq 20mg$ , which in this case seems to be the crossover force [see

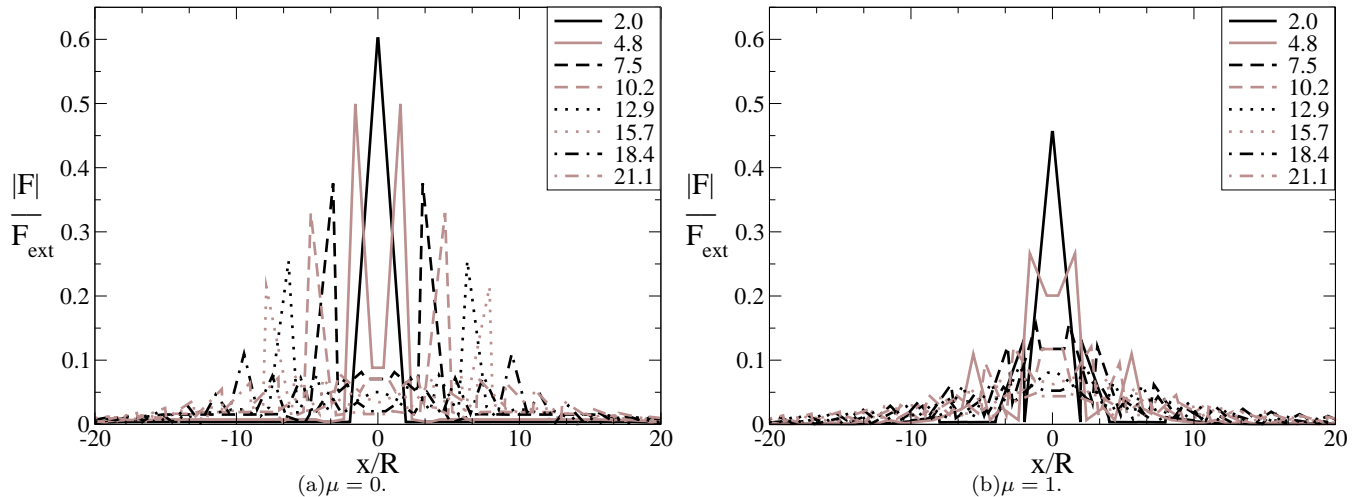


FIG. 15: The norms of the interparticle forces,  $|f|$ , vs. the horizontal position,  $x$ , in ordered systems, with applied force  $F_{\text{ext}} = 150mg$ . The legend indicates the depth measured from point of application of the force, in particle radii (compare to the experimental measurements shown in [18, 22]). (a) Frictionless particles, (b) Frictional particles with  $\mu^{\text{wall}} = \mu = 1$ ,  $k_T/k_N = 0.8$ .

Fig. 16(a)]. Sliding does occur in the system (mainly near the point of application) even for smaller forces, and sliding contacts spread gradually downward with increasing  $F_{\text{ext}}$  (possibly due to the fact that the displacements induced by the applied force decay with the distance from it). It therefore appears that the crossover for  $\mu = 0.2$  is associated with the gradual reduction of the compensating effect of the tangential forces due to sliding. For larger forces ( $F_{\text{ext}} \gtrsim 40mg$ ), a small third peak appear at  $x = 0$  (below the point of application), which appears to be related to a reorganization of the sliding contacts within the “teardrop”.

For  $\mu = 1$ , however, we observe quite a different behavior. As described in Sec. V A, the response remains single peaked (and even becomes sharper) for rather large forces, much beyond those for which the crossover is obtained for  $\mu = 0.2$  [see Fig. 7(b)]. However, when the force exceeds  $F_{\text{ext}} = 91mg$ , we obtain a sharp transition to a very different response shape [see Fig. 16(b)], which is very asymmetric (unlike the symmetric double peaked response obtained for lower friction at large forces). The sign of symmetry breaking appears to be related to the transient vibrations which are excited by the application of the force; for some very close values of the force [e.g.,  $F_{\text{ext}} = 95mg$ , shown in Fig. 16(b)] we obtain almost exactly the same rescaled response reflected with respect to the vertical axis through  $x = 0$ . The shape remains qualitatively similar for much larger  $F_{\text{ext}}$ . The transition to an asymmetric response is accompanied by a significant change in the contact network (which becomes asymmetric), and by a marked *reduction* in the number of sliding contacts.

This instability at large  $\mu$  appears to be dominated by sliding, rather than by changes in the contact network. Its source (and in particular the breaking of symmetry) is

yet unclear, although it may be related to the well-known phenomenon of shear banding. It also bears some similarities to elastic buckling (however, it is clearly outside the linear elastic regime).

## F. A Pile Geometry

While the work presented here is focused on the response of a granular slab, we also examined the effect of friction in a pile composed of 11 layers of monodisperse disks arranged on a triangular lattice, prepared as described in Sec. III C (similar to the frictionless piles studied in [79]). These piles are quite unrealistic, since the sides of the pile are at  $30^\circ$  to the horizontal, which is larger than the realistic angle of repose for disks. Therefore, the edges of the pile have to be supported by side walls (the construction of stable piles on an uncorrugated floor requires the introduction of *rolling friction*, or rolling resistance [87]).

The forces and the corresponding vertical stress component  $\sigma_{zz}$  in the pile are shown in Figs. 17(a)-(d). As in the case of a slab (Figs. 13 and 14), the effect of friction is rather large. In particular, as shown in Figs. 17(c),(d), the pile of frictionless disks exhibits a dip in the stress under the apex, but the pile of frictional disks does not. The dip in the frictionless case is due to the open horizontal contacts in the central region of the pile; see Fig. 17(e). In the frictional case, the size of the region of open contacts in the central region of the pile is quite similar, but its shape is different [Figs. 17(e),(f)]. The absence of the dip results from the reduced anisotropy due to the frictional forces, as discussed above for a slab geometry. We therefore conclude that the presence or absence of a dip in a pile geometry is determined by the degree of



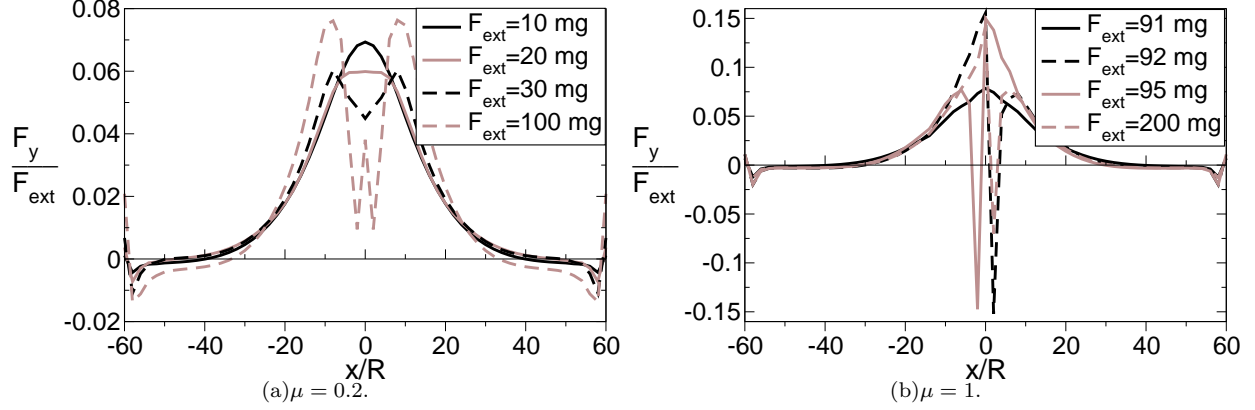


FIG. 16: The response of ordered systems, with different coefficients of friction  $\mu$ , to an applied force ( $F_{\text{ext}}$ ) of different magnitudes, frictionless walls ( $\mu^{\text{wall}} = 0$ ) and  $k_T/k_N = 0.8$ .

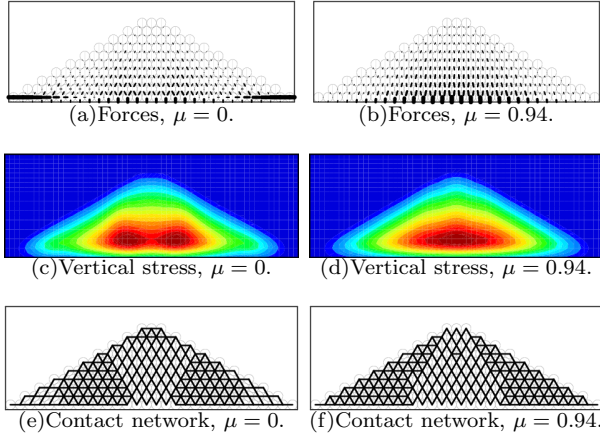


FIG. 17: (a),(b) the interparticle forces in a pile of monodisperse disks under gravity, with and without friction (in the frictional case,  $\mu = 0.94$ ,  $\mu^{\text{wall}} = 0.35$  and  $k_T/k_N = 0.5$ ). Line widths and lengths are proportional to the force magnitude; (c),(d) the vertical stress  $\sigma_{zz}$  in the same systems, calculated using a Gaussian coarse graining function with a coarse graining width  $w = 2R$ ; (e),(f) the contact network: particles in contact are connected by lines.

anisotropy in the *mechanical properties* of the pile (which is not always simply related to the anisotropy of the contact network, as shown here in the frictional case). These properties are expected to depend on the way the pile is prepared, as observed in [15].

### G. Effects of an applied torque

It is interesting to note that the force chains are also sensitive to additional applied torques. Fig. 18 shows the force chains obtained in systems of  $25 \times 13$  slightly polydisperse particles ( $\delta = 10^{-3}$ ) with  $k_T/k_N = 0.5$ ,  $\mu = \mu^{\text{wall}} = 0.5$ , for an applied force  $F_{\text{ext}} = 10\bar{m}g$  at

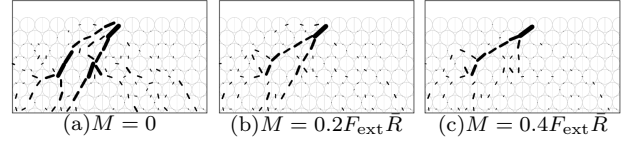


FIG. 18: Force chains in 2D packings of slightly polydisperse frictional particles ( $\delta = 10^{-3}$ ), with a force  $F_{\text{ext}} = 10\bar{m}g$  applied at  $30^\circ$  to the horizontal, and different applied torques in the clockwise direction (indicated below each figure). The effect of gravity has been subtracted. The same realization of the packing was used in all cases. The region shown is the central third of the upper half of the system.

$30^\circ$  to the horizontal, with different applied torques (as may occur if the line of action of an external force applied to a particle does not pass through its center of mass). As shown, additional torques can have quite a large effect on the obtained force chains. Although the effect on the stress field (in particular, its asymmetric part) is typically confined to a region close to the point of application, this may indicate that for some effects it is important to extend the continuum description to incorporate torques and rotations, i.e., use a micropolar or Cosserat continuum model [88, 89, 90]).

## VI. EFFECTS OF DISORDER

While the study of ordered systems of monodisperse grains allows for simpler theoretical modeling, real granular systems are never composed of perfectly identical particles. Even disks of nominally equal sizes (as used, e.g., in [18, 22]) exhibit a certain polydispersity. Most real granular matter exhibits considerable polydispersity (as well as a variability in particle shapes). It is therefore important to verify that the results obtained for monodisperse system, as described above, are not limited to this particular, idealized case. We therefore performed simu-

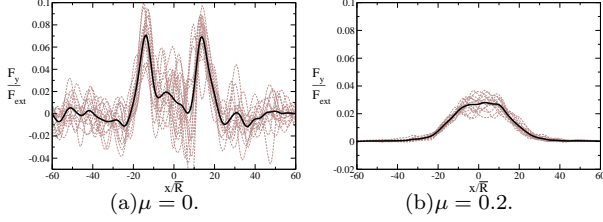


FIG. 19: The response of frictionless and frictional ( $\mu = \mu^{\text{wall}} = 0.2, k_T/k_N = 0.8$ ) disordered systems (with polydispersity  $\delta = 0.01$ ) with  $F^{\text{ext}} = 15\bar{m}g$  ( $\bar{m}$  is the mean particle mass). Thin gray lines correspond to the responses of 15 individual realizations in each case, smoothed with a Gaussian of width  $w = 3\bar{R}$ ; the thick black line corresponds to an average over these 15 configurations.

lations with polydisperse systems (with radii distributed uniformly in the interval  $[R - \delta \cdot R, R]$ ; see Sec. III B, with  $\delta = 0.01, 0.1, 0.25$ ). In general, we find that polydisperse systems exhibit qualitatively similar behavior to the ordered systems described in Sec. V. The effects of polydispersity are described in detail in this section.

Since disorder induces fluctuations (which are not present in ordered systems), the forces were coarse grained using a Gaussian coarse-graining function in the horizontal ( $x$ ) direction:  $\frac{1}{w\sqrt{\pi}}e^{-(x/w)^2}$  with  $w = 3\bar{R}$  or  $w = 6\bar{R}$ , which amounts to calculating the vertical stress  $\sigma_{zz}$  at the floor [91]. The stress was then averaged over several realization of the disorder (typically five).

The effect of friction on the response in disordered systems is qualitatively similar to that found in the ordered lattices described in Sec. V: Fig. 19 presents a comparison of the response (averaged over 15 different realizations, coarse grained with  $w = 3\bar{R}$ ) obtained in frictionless and frictional ( $\mu = 0.2$ ) disordered packings with  $\delta = 0.01$ , with an applied force  $F^{\text{ext}} = 15\bar{m}g$  ( $\bar{m}$  is the mean particle mass). As in the ordered case, the response is very different: there are two very distinct peaks in the frictionless case, but one peak in the frictional case. The fluctuations are quite large even for this small degree of polydispersity (and larger for the frictionless case), but for the magnitude of the applied force used in this case the difference between the frictionless and frictional case is quite evident even for individual realizations.

### A. Linearity and the Crossover Force

A notable difference between monodisperse and polydisperse systems is that in the latter, the range of linear response is smaller (see Fig. 20 compared to Fig. 6).

In order to examine the effects of polydispersity and friction in more detail, we performed similar simulations with different degrees of polydispersity and coefficients of friction  $\mu$ , for different applied forces. The results are depicted in Fig. 21. The larger the coefficient of friction, the larger the applied force at which the crossover from a

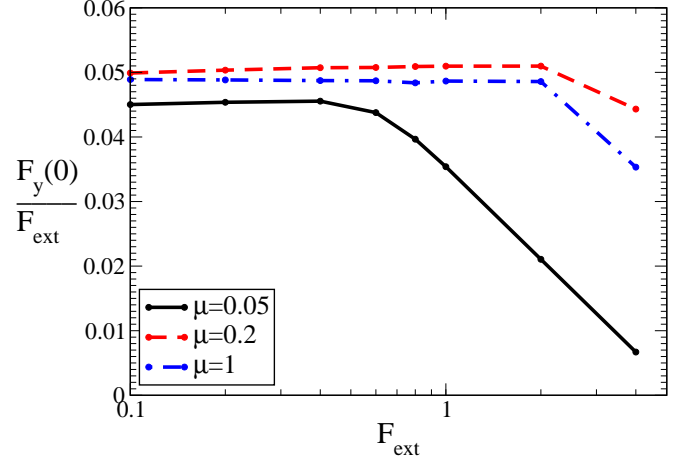


FIG. 20: The response at  $x = 0$  (coarse grained with  $w = 3\bar{R}$ ) of a single polydisperse systems with  $\delta = 0.01$ , normalized by the applied force,  $F_{\text{ext}}$ , vs. the applied force (given in units of the mean particle weight,  $\bar{m}g$ ), for different coefficients of friction  $\mu$ , with frictionless walls ( $\mu^{\text{wall}} = 0$ ) and  $k_T/k_N = 0.8$  (compare to Fig. 6).

single peaked to a double peaked response occurs, much like in ordered systems (Sec. V A. As mentioned above, the crossover force decreases with increasing polydispersity, or disorder. For polydisperse systems we observed a rather gradual crossover even for  $\mu = 1$ , unlike the sharp transition to a highly asymmetric response in lattice configurations [Sec. V E]. A possible explanation may be that for a single disordered realization, the response is not symmetric even for a small external force. In addition, it may be impossible to apply very large forces to polydisperse systems without causing major rearrangements.

It is quite remarkable that an average over a very small ensemble of only five realizations (with coarse graining) is sufficient to demonstrate the crossover from a single peak to a double peak, and even results (in some cases) in nearly symmetrical graphs. It appears that, at least when the force is not too close to its crossover value, the fluctuations within the ensemble are rather small for this choice of coarse graining length (see [91] for a detailed study of another set of simulations in the linear force regime), so that the typical response of a realization resembles that of the ensemble average.

The results for different degrees of polydispersity (including the case of a lattice) can be summarized in a schematic phase diagram, Fig. 22 [1]. Note that in our simulations a specific preparation method has been used: relaxation under gravity from a near-lattice configuration, so that (at least for small  $\delta$ ), the configuration retains partial order. In the range of polydispersity studied here, more disordered systems exhibit a smaller crossover force, i.e., they are more susceptible to induced anisotropy. It is possible that this result pertains to small polydispersity and a larger polydispersity may actually stabilize the system. In the systems studied here, the dis-



tribution of contact angles may not be quite isotropic, exhibiting preferred direction close to those of the triangular lattice, and therefore more susceptible to failure along certain direction. Therefore, in more disordered systems, the degree of induced anisotropy may be smaller, yielding a non-monotonic dependence of the crossover force on the degree of polydispersity. In any case, it is likely that the crossover does not depend on the polydispersity alone but also on the preparation method (as observed in experiments on granular piles [15] and slabs [20]). A more complete phase diagram would presumably further depend on additional parameters which characterize the geometry of the packing (in a statistical way). A common approach is to use fabric tensors [92], often simplified by considering the distribution of contact angles. However, this characterization is often employed in conjunction with a mean-field approach, which fails for disordered granular materials [93, 94] due to the large non-affine component of the microscopic displacements (see also [85]).

### B. Superposition

Another issue related to the question of linearity, discussed in Sec. VI A, is that of superposition: is the sum of responses to several forces applied individually the same as the response to all the forces applied at the same time?

Fig. 23 demonstrates a typical superposition test. Here, two downward pointing vertical forces, each of magnitude  $F_{\text{ext}} = 0.2\bar{m}g$ , are applied at two points at the top of the slab, otherwise characterized by  $\delta = 1\%$  and  $\mu = 0.05$ , for which the linear range is rather small ( $F_{\text{ext}} \lesssim 0.4\bar{m}g$ ). We compared the response of the system when each of the forces was applied separately and simultaneously at different horizontal separations. As shown in Fig. 23, superposition holds even on the *microscopic scale*, i.e., for individual forces without coarse graining.

Interestingly, we find that superposition holds quite well even beyond the linear regime, as shown in Fig. 24 (for  $F_{\text{ext}} = \bar{m}g$ ). A possible reason is that sufficiently far from where the forces are applied, the rearrangements (changes in the contact network or sliding) are less sensitive to the precise positions of the applied forces. In more general terms, it is possible that the response to a distribution of forces, sufficiently far from the region where they are applied, is not very sensitive to the details of the distribution.

This explanation is similar to St. Venant’s principle (see, e.g., [95]), which states (for a *linear elastic* system) that the difference in stresses and strains in the interior of an elastic body due to two separate but statically equivalent systems of surface tractions (same overall force and torque), are negligible sufficiently far from the area where the loads are applied. In the case considered here, the system is certainly not strictly elastic for  $F_{\text{ext}} \gtrsim 0.4\bar{m}g$  (due to the effects of contact network changes and sliding). However, the response to a localized force (in an elastic medium) decays with the distance

from the point of application as a power law (e.g., the solutions for an infinite half plane or half space [Boussinesq’s problem], which decay like  $1/z$  in 2D and  $1/z^2$  in 3D [28, 53]). Therefore, as the distance from the point of application increases, the relative displacements of the particles become smaller, and they are less likely to reach the nonlinear regime (the finite region of open contacts discussed in Sec. V is an example of such a nonlinear effect), so that far from the point of application of the force, the system becomes “more elastic” and the response to a distributed load is the same (or nearly the same) as the response to the resultant load. This suggestion may apply to recent experiments [96, 97] on a 2D system subject to a small cyclic displacement, which shows a  $1/r$  decay of the displacement field at large distances from the perturbation.

## VII. INTERPRETATION OF EXPERIMENTAL RESULTS

The results described in the previous section help to interpret the experimental results reviewed in Sec. II B. To this end, it is important to note that the different experiments described in Sec. II B correspond to different regions of the phase diagram [Fig. 22] described in Sec. VI.

As mentioned, experiments on 2D systems using photoelastic particles [18, 22] typically use a rather large applied force ( $F_{\text{ext}} \simeq 150mg$  in these experiments), required in order to obtain a significant photoelastic effect. In these experiments the interparticle forces, rather than the macroscopic stress, were measured (the forces on the floor have not been measured). These are reproduced quite well by our DEM simulations with friction (see Sec. V). It is yet unclear whether these experiments are compatible with the phase diagram of Sec. VI, since the macroscopic stress has not been measured directly in these experiments.

The experiments reported in [19, 20] used disordered systems with a rather small applied force (a few times the particle weight), for which a single peak was observed, in agreement with the phase diagram. Since these experiments used sand, rather than spherical particles, the effective coefficient of static friction may be much larger than 1, so that sliding is less likely to occur. Note that those experiments were performed on a 3D system, while the simulations reported here are in 2D; however, we expect similar qualitative features of the phase diagram in 3D systems. The difference in the responses of dense and loose sand [20], as well as the deviations from the isotropic elastic prediction observed in both cases, may be explained by a (small) anisotropy, induced by the packing construction process (see also [98]). We believe that the anisotropy induced by the small applied force in these experiments should be negligible (note that the systems studied in [19, 20] are also deeper, in terms of particle diameters, than the ones studied in [18, 22]).

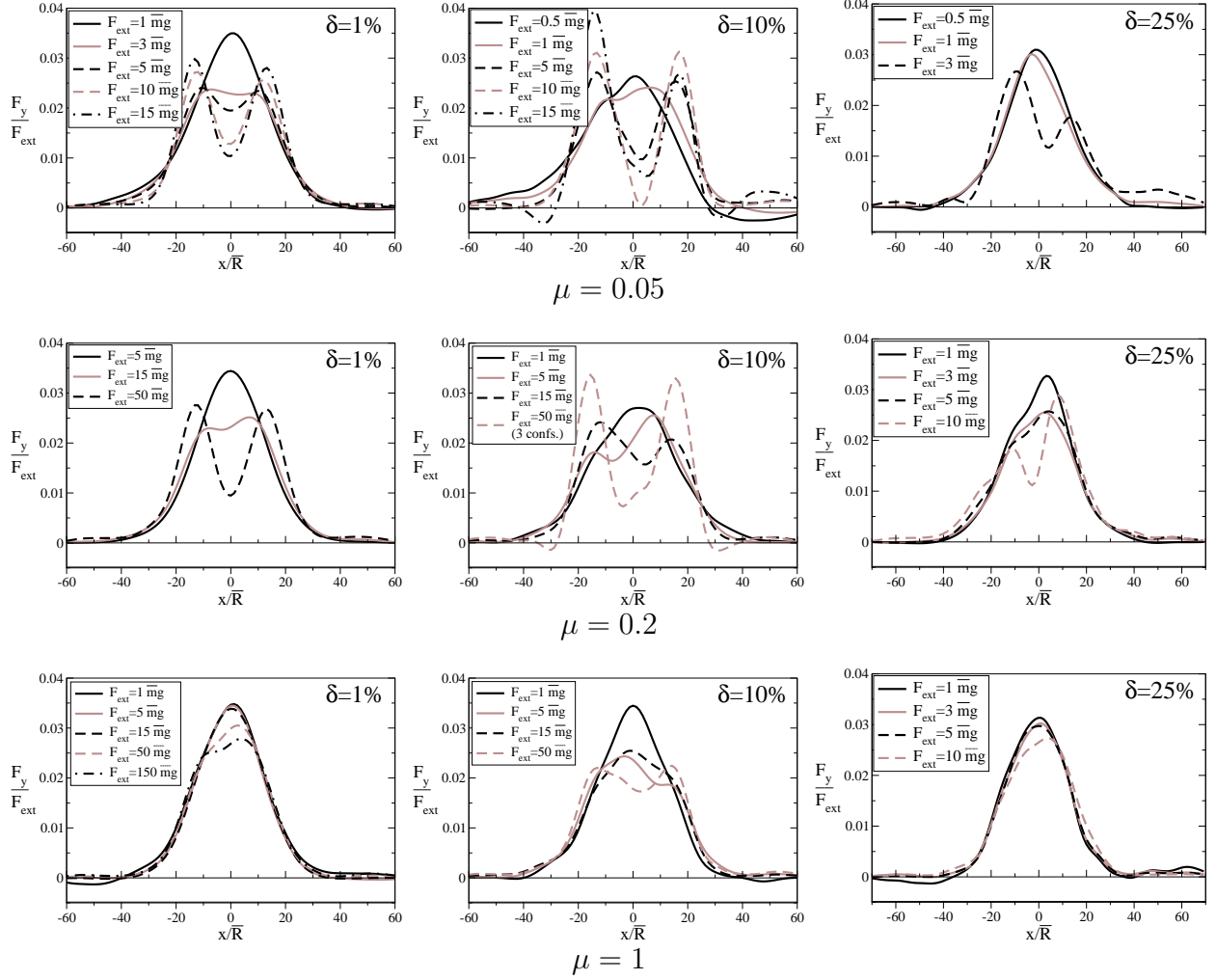


FIG. 21: The response of disordered systems with different degrees of polydispersity,  $\delta$ , and coefficients of friction, ( $\mu = \mu^{\text{wall}}$ ), with  $k_T/k_N = 0.8$ , to different applied forces  $F_{\text{ext}}$ . The response is averaged over 5 configurations (3 for the largest force used with  $\delta = 10\%$  and  $\mu = 0.2$ , for which the system was unstable) and smoothed with a Gaussian of width  $w = 6\bar{R}$ .

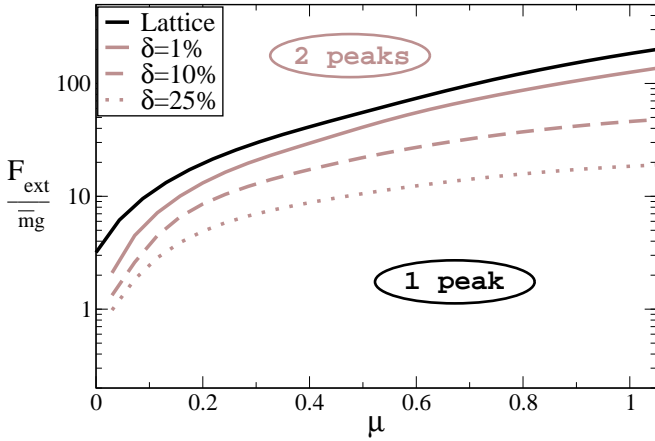


FIG. 22: Schematic phase diagram (in the  $F_{\text{ext}}-\mu$  plane) for the crossover from a single peaked to a double peaked response, with different degrees of polydispersity.

In contrast to the experiments reported in [19, 20], the experiments reported in [21] on ordered 3D packings used a very large force of a few thousand times the particle weights. Several distinct peaks were observed for shallow systems. These peaks became more diffuse for deeper systems. In the absence of horizontal contacts, the coordination number in the HCP and FCC lattice is reduced to 6 (each particle is in contact with 3 particles in the layer above it and that below it). This corresponds to the isostatic limit (in the absence of friction). Apparently, the experimentalists attempted to avoid horizontal contacts by choosing the appropriate wall spacing; even if some horizontal contacts were present, it is likely that such a large force opened the horizontal contacts, at least in the top layers. Since the force is large, it may also lead to sliding at most of the contacts (at least in the top layers), so that for shallow systems, the observed behavior is extremely anisotropic, and, as mentioned, near the isostatic limit. However, in deeper systems, the opening of

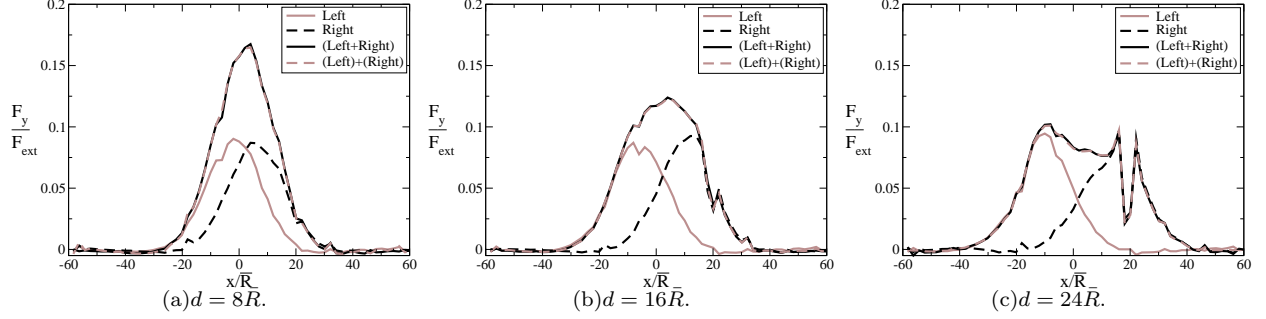


FIG. 23: Superposition in a polydisperse system with  $\delta = 0.01$ ,  $\mu = 0.05$ , and  $F_{\text{ext}} = 0.2\bar{m}g$ , frictionless walls ( $\mu^{\text{wall}} = 0$ ) and  $k_T/k_N = 0.8$ .  $d$  indicates the distance between the points of application of the two forces (applied symmetrically with respect to the center top particle), given in mean particle diameters  $\bar{R}$ . In the legend, **Left** denotes the response to a force applied to the left of the center particle, **Right** to a force applied to its right, **(Left+Right)** to the two forces applied together and **(Left)+(Right)** the sum of **Left** and **Right**. The results shown are for the individual forces (no coarse graining) in a single realization.

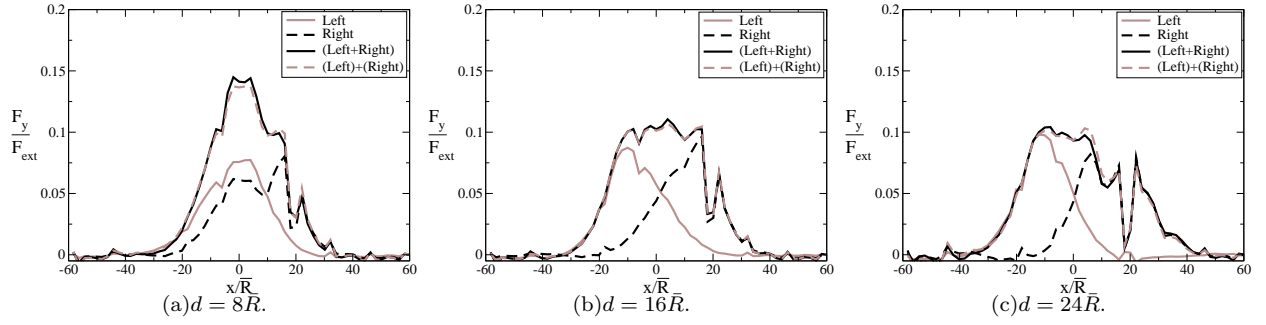


FIG. 24: Superposition in a polydisperse system with  $\delta = 0.01$ ,  $\mu = 0.05$ , and  $F_{\text{ext}} = \bar{m}g$  (same as Fig. 23 with a different applied force; the same realization of the disorder was used).

contacts and sliding may be reduced (as we observed for  $\mu = 0.2$ ), reducing the anisotropy (note that even the deepest layers in the described experiment were not very deep: about 20 layers). In amorphous packings, a single peak was observed (however, the method of application of the force was different: a force impulse was used, which may correspond to a weaker force in our quasi-static description). Thus, the results of the experiments reported in [21] are also consistent with the schematic phase diagram presented in Sec. VI.

The phase diagram may also explain the striking difference observed in [23] between the experimentally measured displacement response in packings of (frictional) disks subject to a localized displacement (which exhibits a single peak), and the results of simulations of frictionless isostatic packings (which exhibits two peaks). Note, however, that the mean coordination number in the frictionless polydisperse systems studied here (e.g.,  $z \sim 4.25$  for  $\delta = 0.01$ ) is well above the isostatic limit of  $z = 4$ . It is, however, much smaller than that of the ideal triangular lattice,  $z = 6$ , the “missing” contacts being predominantly horizontal. This suggests that the anisotropic (“hyperbolic-like”) response of frictionless systems may arise, at least for small polydispersity,

from the anisotropic structure of these systems rather than their (near)-isostaticity, as suggested in [23].

## VIII. CONCLUDING REMARKS

We performed simulations studying the response of a 2D granular slab to a localized force, in particular the effects of the magnitude of the applied force, the frictional parameters and the polydispersity. Our results indicate that *anisotropy*, which is induced by changes in the contact network and frictional sliding due to applied force, gives rise to a hyperbolic-like response (as already suggested in [3, 25]). However, we show that this effect becomes less pronounced for large systems (which is more likely to be the case in most engineering applications) and/or systems subject to smaller applied forces for a given system size. This may explain why small-scale experiments sometimes yield a hyperbolic-like response while elasticity is typically used for describing small deformations in engineering practice. In addition, *friction*, which is present in all real granular systems, increases the range of linearity in the applied force and further reduces the effect of stress-induced anisotropy,

rendering the response even closer to that predicted by isotropic elasticity. The same behavior is observed in polydisperse systems, which is the typical case in nature, although in polydisperse systems the forces at which induced anisotropy becomes large are smaller. The validity of superposition beyond the linear elastic regime indicates that sufficiently far from the applied load, the system responds (nearly) elastically even though it is not elastic everywhere.

The above considerations should also be relevant for the case of granular piles, whose properties depend strongly on their construction history [15]. For instance, when the pile is grown from a point source, it is shaped by successive avalanches, all of which are initiated in the apex area (beneath the source). The nature of the granular flow (i.e., the avalanches) in the case of formation by flow from an extended source is clearly different from that corresponding to a point source. In particular, the degree of anisotropy of piles constructed from a point source is larger than that of piles built from an extended (and approximately uniform) source [99]. In the former case, there is a dip in the pressure distribution on the floor, whereas in the latter there is no dip. In [15], this effect was described in terms of orientations of force chains, which may also reflect the macroscopic anisotropy. However, we believe that once the (possibly inhomogeneous) anisotropy in the pile is taken into account, the stress distribution under the pile should be compatible with an elastic picture. The question of how this anisotropy is created during construction will probably require a more detailed description of the pile dynamics, possibly involving the changes in the contact network (and sliding) which lead to macroscopic anisotropy.

In general, the elastic description of granular solids is expected to be valid for sufficiently large scales (and system sizes) and not-too-large applied forces. Outside this range, such a description may need to be extended by using a nonlinear, incrementally elastic continuum model, with stress-history dependent elastic moduli (which re-

flect the induced anisotropy, and may exhibit hyperbolic-like behavior). The nonlinear effects of broken contacts and frictional sliding should be important in understanding the failure of granular materials. In particular, the dominant effect of tangential forces in such failure, e.g., in the transition to an asymmetric response described in Sec. V E, as well as the effects of applied torques (Sec. V G) and of rolling resistance, support the suggestion that, at least on intermediate scales, continuum models of micropolar, or Cosserat type [88, 89, 90] may be required (see, e.g., [100, 101]).

We note, as a suggestion for a future experiment, that one should be able to observe experimentally the crossover we obtain in the simulations with increasing applied force, from a single peaked to a double peaked response; in such an experiment, the setup should be sufficiently sensitive to measure the response to a small force (in the linear regime) but also sufficiently robust to enable the application of larger forces. In addition, the force would have to be applied slowly, to avoid plastic flow of the material. Such an experiment would be very useful in testing the applicability of the above physical considerations to real granular materials.

### Acknowledgments

We thank A. P. F. Atman, R. P. Behringer, P. Claudin, E. Clément, J. Geng, N. Mueggenburg, M. van Hecke, W. van Saarloos and T. A. Witten for useful discussions. We gratefully acknowledge support from the Israel Science Foundation (ISF), grant no. 689/04, the German-Israeli Science Foundation (GIF), grant no. 795/2003 and the US-Israel Binational Science Foundation (BSF), grant no. 2004391. CG acknowledges financial support from a Chateaubriand Fellowship and from a European Community FP6 Marie Curie Action (MEIF-CT2006-024970).

- 
- [1] C. Goldenberg and I. Goldhirsch, *Nature* **435**, 188 (2005).
  - [2] R. M. Nedderman, *Statics and Kinematics of Granular Materials* (Cambridge University Press, 1992).
  - [3] S. B. Savage, in *Proceedings of the NATO Advanced Study Institute on Physics of Dry Granular Media, Cargèse, France, September 15-26, 1997*, edited by H. J. Herrmann, J. P. Hovi, and S. Luding (Kluwer, 1998), pp. 25–95.
  - [4] W. Wu, E. Bauer, and D. Kolymbas, *Mech. Mat.* **23**, 45 (1996).
  - [5] G. Gudehus and K. Nubel, *Geotechnique* **54**, 187 (1979).
  - [6] J. P. Wittmer, M. E. Cates, and P. Claudin, *J. de Physique I* **7**, 39 (1997).
  - [7] A. V. Tkachenko and T. A. Witten, *Phys. Rev. E* **60**, 687 (1999).
  - [8] D. A. Head, A. V. Tkachenko, and T. A. Witten, *Eur. Phys. J. E* **6**, 99 (2001).
  - [9] S. F. Edwards and D. V. Grinev, *Physica A* **302**, 162 (2001).
  - [10] R. C. Ball and R. Blumenfeld, *Phys. Rev. Lett.* **88**, 115505 (2002).
  - [11] R. Blumenfeld, *Phys. Rev. Lett.* **93**, 108301 (2004).
  - [12] J.-P. Bouchaud, P. Claudin, M. E. Cates, and J. P. Wittmer, in *Proceedings of the NATO Advanced Study Institute on Physics of Dry Granular Media, Cargèse, France, September 15-26, 1997*, edited by H. J. Herrmann, J. P. Hovi, and S. Luding (Kluwer, 1998), pp. 97–135.
  - [13] J. Smid and J. Novosad, in *Proceedings of the 1981 Powtech Conference, Institution of Chemical Engineers Symposium* (1981), vol. 63, pp. D3V 1–12.
  - [14] R. Brockbank, J. M. Huntley, and R. C. Ball, *J. de*

- Physique II **7**, 1521 (1997).
- [15] L. Vanel, D. Howell, D. Clark, R. P. Behringer, and E. Clément, Phys. Rev. E **60**, R5040 (1999).
  - [16] P. G. de Gennes, Rev. Mod. Phys. **71**, S374 (1999).
  - [17] M. Da Silva and J. Rajchenbach, Nature **406**, 708 (2000).
  - [18] J. Geng, D. Howell, E. Longhi, R. P. Behringer, G. Reydellet, L. Vanel, E. Clément, and S. Luding, Phys. Rev. Lett. **87**, 035506 (2001).
  - [19] G. Reydellet and E. Clément, Phys. Rev. Lett. **86**, 3308 (2001).
  - [20] D. Serero, G. Reydellet, P. Claudin, E. Clément, and D. Levine, Eur. Phys. J. E **6**, 169 (2001).
  - [21] N. W. Mueggenburg, H. M. Jaeger, and S. R. Nagel, Phys. Rev. E **66**, 031304 (2002).
  - [22] J. Geng, G. Reydellet, E. Clément, and R. P. Behringer, Physica D **182**, 274 (2003).
  - [23] C. F. Moukarzel, H. Pacheco-Martínez, J. C. Ruiz-Suarez, and A. M. Vidales, Granular Matter **6**, 61 (2004).
  - [24] Y. Jiang and M. Liu, Eur. Phys. J. E **22**, 255 (2007).
  - [25] M. E. Cates, J. P. Wittmer, J.-P. Bouchaud, and P. Claudin, Chaos **9**, 511 (1999).
  - [26] A. Kasahara and H. Nakanishi, Phys. Rev. E **70**, 051309 (2004).
  - [27] S. Ostojic and D. Panja, Phys. Rev. Lett. **97**, 208001 (2006).
  - [28] L. Landau and E. Lifshitz, *Theory of Elasticity, 3rd Edition* (Pergamon, Oxford, 1986).
  - [29] C. Goldenberg and I. Goldhirsch, Phys. Rev. Lett. **89**, 084302 (2002).
  - [30] P. Claudin, J.-P. Bouchaud, M. E. Cates, and J. P. Wittmer, Phys. Rev. E **57**, 4441 (1998).
  - [31] C. F. Moukarzel, Phys. Rev. Lett. **81**, 1634 (1998).
  - [32] J.-N. Roux, Phys. Rev. E **61**, 6802 (2000).
  - [33] C. F. Moukarzel, Granular Matter **3**, 41 (2001).
  - [34] J.-P. Bouchaud, P. Claudin, D. Levine, and M. Otto, Eur. Phys. J. E **4**, 451 (2001).
  - [35] J. E. S. Socolar, D. G. Schaeffer, and P. Claudin, Eur. Phys. J. E **7**, 353 (2002).
  - [36] M. Otto, J.-P. Bouchaud, P. Claudin, and J. E. S. Socolar, Phys. Rev. E **67**, 031302 (2003).
  - [37] Y. Roichman, D. Levine, and I. Yavneh, Phys. Rev. E **70**, 061301 (2004).
  - [38] S. Alexander, Phys. Reports **296**, 65 (1998).
  - [39] D. W. Howell and R. P. Behringer, Chaos **9**, 559 (1999).
  - [40] C.-H. Liu, S. R. Nagel, D. A. Schecter, S. N. Copper-smith, S. Majumdar, O. Narayan, and T. A. Witten, Science **269**, 513 (1995).
  - [41] S. N. Coppersmith, C.-H. Liu, S. Majumdar, O. Narayan, and T. A. Witten, Phys. Rev. E **53**, 4673 (1996).
  - [42] C. Kittel, *Introduction to Solid State Physics* (Wiley, 1956).
  - [43] P. A. Cundall and O. D. L. Strack, Geotechnique **29**, 47 (1979).
  - [44] P. A. Cundall, A. Drescher, and O. D. L. Strack, in *IUTAM Conference on Deformation and Failure of Granular Materials, Delft, Holland, 31 August - 3 September 1982*, edited by P. A. Vermeer and H. J. Luger (1982), pp. 355–369.
  - [45] M. P. Allen and D. J. Tildesley, *Computer simulation of liquids* (Oxford University Press, Oxford, 1987).
  - [46] D. Frenkel and B. Smit, *Understanding Molecular Simulations* (Academic Press, San Diego, 1996).
  - [47] D. C. Rapaport, *The Art of Molecular Dynamics Simulation* (Cambridge University Press, Cambridge, 1997).
  - [48] R. J. Sadus, *Molecular Simulation of Fluids: Theory, Application and Object-Orientation* (Elsevier, Amsterdam, 1999).
  - [49] D. E. Wolf, in *Computational Physics*, edited by K. H. Hoffmann and M. Schreiber (Springer, Heidelberg, 1996), pp. 64–94.
  - [50] H. J. Herrmann and S. Luding, Cont. Mech. and Thermodynamics **10**, 189 (1998).
  - [51] H. Zhu, Z. Zhou, R. Yang, and A. Yu, Chem. Eng. Sci. **62**, 3378 (2007).
  - [52] G. M. L. Gladwell, *Contact Problems in the Classical Theory of Elasticity* (Sijthoff & Noordhoff, The Netherlands, 1980).
  - [53] K. L. Johnson, *Contact Mechanics* (Cambridge University Press, Cambridge, 1985).
  - [54] T. Pöschel and V. Buchholtz, Phys. Rev. Lett. **71**, 3963 (1993).
  - [55] O. R. Walton and R. L. Braun, in *Joint DOE/NSF Workshop on Flow of Particulates and Fluids* (1993).
  - [56] T. Pöschel and V. Buchholtz, J. de Physique I **5**, 1431 (1995).
  - [57] H. G. Matuttis, S. Luding, and H. J. Herrmann, Powder Technology **109**, 278 (1999).
  - [58] L. Vu-Quoc, X. Zhang, and O. R. Walton, Computer Methods in Applied Mechanics and Engineering **187**, 483 (2000).
  - [59] A. Schinner, Granular Matter **3**, 35 (2001).
  - [60] J. Schäfer, S. Dippel, and D. E. Wolf, J. de Physique I **6**, 5 (1996).
  - [61] M. H. Sadd, Q. Tai, and A. Shukla, Int. J. Non-Linear Mech. **28**, 251 (1993).
  - [62] O. R. Walton, in *Mobile Particulate Systems*, edited by E. Guazzelli and L. Oger (Kluwer, Dordrecht, 1995), pp. 367–380.
  - [63] J. Schwartz and E. Y. Harper, Int. J. Solids Struct. **7**, 1613 (1971).
  - [64] T. Schwager, Phys. Rev. E **75**, 051305 (2007).
  - [65] T. S. Majmudar, M. Sperl, S. Luding, and R. P. Behringer, Phys. Rev. Lett. **98**, 058001 (2007), Supplementary Information.
  - [66] N. V. Brilliantov, F. Spahn, J.-M. Hertzsch, and T. Pöschel, Phys. Rev. E **53**, 5382 (1996).
  - [67] L. Vu-Quoc and X. Zhang, Mech. Mat. **31**, 235 (1999).
  - [68] L. Pournin, T. M. Liebling, and A. Mocellin, Phys. Rev. E **65**, 011302 (2001).
  - [69] J. Krim, Am. J. Phys. **70**, 890 (2002).
  - [70] E. Rabinowicz, J. App. Phys. **22**, 1373 (1951).
  - [71] R. J. Bathurst and L. Rothenburg, J. Appl. Mech. **55**, 17 (1988).
  - [72] C. S. Chang and J. Gao, Acta Mechanica **115**, 213 (1996).
  - [73] J. T. Jenkins and L. L. Ragione, Int. J. Solids Struct. **38**, 1063 (2001).
  - [74] C. Gay and R. da Silveira, Europhys. Lett. **68**, 51 (2004).
  - [75] L. Brendel and S. Dippel, in *Proceedings of the NATO Advanced Study Institute on Physics of Dry Granular Media, Cargèse, France, September 15-26, 1997*, edited by H. J. Herrmann, J. P. Hovi, and S. Luding (Kluwer, 1998), pp. 313–318.
  - [76] J. Geng and R. P. Behringer, private communication.

- [77] J. W. Landry and G. S. Grest, Phys. Rev. E **69**, 031303 (2004).
- [78] A. P. F. Atman and P. Claudin, in *Proc. Traffic and Granular Flow 2003*, edited by S. P. Hoogendoorn, S. Luding, P. H. L. Bovy, M. Schreckenberg, and D. Wolf (Springer-Verlag, 2005), pp. 531–536, cond-mat/0310564.
- [79] S. Luding, Phys. Rev. E **55**, 4720 (1997).
- [80] M. Oda, Mech. Mat. **16**, 35 (1993).
- [81] I. Goldhirsch and C. Goldenberg, in *The Physics of Granular Media*, edited by H. Hinrichsen and D. E. Wolf (Wiley-VCH, 2004), pp. 3–22.
- [82] J. Duffy and R. D. Mindlin, J. Appl. Mech. **24**, 585 (1957).
- [83] C. S. Chang and L. Ma, Int. J. Solids Struct. **29**, 1001 (1992).
- [84] R. da Silveira, G. Vidalenc, and C. Gay, cond-mat/0208214.
- [85] I. Goldhirsch and C. Goldenberg, Eur. Phys. J. E **9**, 245 (2002).
- [86] C. Goldenberg and I. Goldhirsch, Granular Matter **6**, 87 (2004).
- [87] Y. C. Zhou, B. D. Wright, R. Y. Yang, B. H. Xu, and A. Yu, Physica A **269**, 536 (1999).
- [88] E. Kröner, ed., *Mechanics of Generalized Continua - Proceedings of the IUTAM-Symposium on the Generalized Cosserat Continuum and the Continuum Theory of Dislocations with Applications* (Springer-Verlag, Freudensstadt and Stuttgart, 1967).
- [89] W. Jaunzemis, *Continuum Mechanics* (MacMillan, New York, 1967).
- [90] A. C. Eringen, in *Fracture: An Advanced Treatise, Volume II: Mathematical Fundamentals*, edited by H. Liebowitz (Academic Press, New York and London, 1968), pp. 621–729.
- [91] C. Goldenberg, A. P. F. Atman, P. Claudin, G. Combe, and I. Goldhirsch, Phys. Rev. Lett. **96**, 168001 (2006).
- [92] K.-I. Kanatani, Int. J. Solids Struct. **22**, 149 (1984).
- [93] C. S. Chang and C. L. Liao, Applied Mechanics Review **47**, 197 (1994).
- [94] H. A. Makse, N. Gland, D. L. Johnson, and L. M. Schwartz, Phys. Rev. Lett. **83**, 5070 (1999).
- [95] G. E. Mase, *Theory and Problems of Continuum Mechanics* (McGraw-Hill, 1970).
- [96] E. Kolb, J. Cviklinski, J. Lanuza, P. Claudin, and E. Clément, Phys. Rev. E **69**, 031306 (2004).
- [97] E. Kolb, C. Goldenberg, S. Inagaki, and E. Clément, J. Stat. Mech.: Theory and Exp. **2006**, P07017 (2006).
- [98] A. P. F. Atman, P. Brunet, J. Geng, G. Reydellet, G. Combe, P. Claudin, R. P. Behringer, and E. Clément, J. Phys. Cond. Mat. **17**, S2391 (2005).
- [99] J. Geng, E. Longhi, R. P. Behringer, and D. W. Howell, Phys. Rev. E **64**, 060301(R) (2001).
- [100] R. de Borst and L. J. Sluys, Comput. Meth. Appl. Mech. Eng. **90**, 805 (1991).
- [101] S. D. C. Walsh and A. Tordesillas, Granular Matter **6**, 27 (2004).